and her mother, both of whom are heterozygous for the S186L mutation, were able to induce *IFNB1* and *IL6* mRNAs after LPS stimulation (Figure 3E), suggesting that the S186L *TRIF* mutation does not affect the TLR4-dependent induction of antiviral IFNs. The induction of *IFNB1* mRNA was variable among controls and subjects, but P1 was the only patient for whom no induction was observed. Consistent with this observation, results from a genome-wide transcriptional analysis of the TLR4 pathway in PBMCs of a control, P1, and an AR MyD88-deficient patient showed impaired responses to LPS in P1 (Supplemental Figure 5A), although P1 responded normally to the TLR7/8 ligand R848 unlike the MyD88-deficient cells (Supplemental Figure 5B). As expected, MyD88-deficient cells did not respond normally to LPS, and a different pattern of LPS dysregulation was observed in the MyD88-deficient cells when compared with that in cells from P1, demonstrating the distinct pathways involved in the TLR4-MyD88 dependent pathway (Supplemental Figure 5, A and C). We found that the functional pathways regulated by LPS in control PBMCs consisted of genes involved in the production of various cytokines (*IFNB1*, *IL23A*, *IL19*, *IL1A*, and *IL1F9*), chemokine-related genes (*CCR1*, *CCL3L1*, *CCL3L3*, *CCL14*, *CCL20*, and *CCL23*), and IFN-regulated genes (*IFIT3* and *IRF8*) (Supplemental Figure 5C). The nonsense mutation in P1 is consistent with a null mutation affecting all aspects of TRIF-specific signaling, including TLR4-TRIF responses. By contrast, the collective data for the kindred carrying a missense TRIF allele point to a specific defect in the TLR3 signaling pathway, suggesting that the TRIF missense allele is dysfunctional and dominant for TLR3 but not TLR4 responses and for the induction of antiviral IFNs in particular.

Impaired cellular responses to viruses. We then assessed the responses of fibroblasts to viral infection. P1 and P2 cells showed impaired production of IFN-β, IFN-λ1/3, and IL-6 upon infection with VSV and HSV-1, like UNC-93B–deficient cells and unlike control cells ($P < 0.05$ for all comparisons) (Figure 4, A and D). Cell viability after infection with VSV and HSV-1 was tested in the presence and absence of exogenous IFN-α (Figure 4, B and E). In control cells, there was a small decrease or no decrease in the number of living cells upon infection with VSV or HSV-1, respectively. However, cells from P1 and P2 both had significantly lower percentages of surviving cells as compared with those of control cells, at MOIs of 10–100 with VSV ($P < 0.05$ for all comparisons) and upon HSV-1 infection ($P < 0.05$ for all comparisons). However, the addition of exogenous IFN-α resulted in very little cell death in cells from either P1 or P2, in contrast with what was observed for STAT1-deficient cells, which were unable to respond normally to IFN-α. This is consistent with the higher VSV viral titers in P1 and P2 compared with those in a healthy control ($P < 0.05$ for both comparisons), which were reduced to control levels after pretreatment with IFN-α (Figure 4C). Similarly, both P1 and P2 showed higher levels of HSV-1 replication compared with those of a control, which was also reduced with the addition of IFN-α (Figure 4F). Thus, the susceptibility of P1 and P2 to viruses probably results from a lack of protective endogenous IFN-α/β and/or IFN-λ production during viral infection. These data suggest that both P1 and P2 harbor a specific defect in the TLR3-dependent induction of IFN-β and IFN-λ, in response to HSV-1 and VSV, resulting in enhanced viral growth and cell death, at least in fibroblasts. This phenotype is consistent with those reported for both UNC-93B and TLR3 deficiencies and suggests that the R141X and S186L *TRIF* alleles are deleterious, with complete cellular penetrance but incomplete clinical penetrance (10, 11).

Functional characterization and complementation of the R141X mutation. We further investigated the impact of the R141X nonsense mutation by transiently transfecting 293HEK-TLR3 cells, which are responsive to poly(I:C) stimulation, with WT, R141X, or ΔNC TRIF constructs. The ΔNC TRIF construct encodes a truncated dominant-negative TRIF, consisting of only the 162 amino acids of the TIR domain (20). As expected, the R141X TRIF plasmid did not induce expression from the IFN-β or NF-κB promoters, unlike the WT plasmid, as shown by luciferase assays (Figure 5A). The level of induction was similar to that of cells transfected with empty plasmids, consistent with a null allele, and contrasting with the dominant-negative effect observed with the ΔNC plasmid. When the cells were transfected with equal amounts of WT plasmid and R141X or ΔNC, lower levels of luciferase activity were observed only in WT/ΔNC cells, suggesting that the R141X allele does not exert a dominant-negative effect. By contrast to what was observed with cells from P1, analysis of the proteins produced by transfected cells revealed the presence of an approximately 15-kDa truncated R141X protein (Figure 5B). The induction of the IFN-β promoter in response to LPS is strictly TRIF dependent. We therefore transiently transfected LPS-responsive 293HEK-TLR4-MD2-CD14 cells with the TRIF plasmids (Figure 5C). The R141X plasmid, unlike the WT plasmid, did not induce luciferase gene expression from the IFN-β plasmid, and cotransfection with the WT plasmid did not decrease luciferase induction, consistent with a null effect. However, the R141X and mock plasmids were able to induce NF-κB after LPS stimulation in these cells, as the induction of the NF-κB promoter is primarily MyD88 dependent, consistent with the known role of TRIF in TLR4 signaling. Transient transfection of control fibroblasts or fibroblasts from the patient with WT TRIF cDNA led to rapid apoptosis (data not shown), as previously shown in other systems (33, 34). Complementation of the patient's fibroblast phenotype was therefore achieved by retroviral transduction. A doxycycline-regulated *TRIF* expression vector was used for the retroviral transduction of fibroblasts from P1, such that *TRIF* expression was repressed in the presence of doxycycline, making it possible to obtain stably transduced clones (Supplemental Figure 6A). The transduction of cells from P1 with the WT TRIF plasmid (P1+WT) restored poly(I:C)-induced IFN-β, IFN-λ, and IL-6 production, whereas cells transduced with the R141X plasmid (P1+R141X) remained unresponsive (Figure 5D). Viral replication after HSV-1 infection was also rescued in P1+WT cells but not in P1+R141X cells (Figure 5E). Thus, the R141X mutation in P1 is responsible for TRIF deficiency and the abolition of TLR3 signaling as well as susceptibility to HSV-1.

Functional characterization of the S186L mutation in 293-TLR3 cells. The molecular mechanism by which the S186L *TRIF* mutation exerts its deleterious effects was then investigated. We transfected 293-TLR3 cells with expression plasmids encoding WT or S186L TRIF. Reporter assays were performed with the IFN-β and NF-κB–luciferase constructs. In WT and S186L *TRIF*-transfected cells, marked induction of IFN-β and NF-κB luciferase was observed in the absence of poly(I:C) stimulation, consistent with previous reports in which *TRIF* overexpression led to TLR3-independent activation of IFN-β and NF-κB (Figure 6A, Supplemental Figure 7A, and refs. 21, 25). We assessed the ability of these mutations to interact with TLR3 upon poly(I:C) stimulation by transfecting 293-TLR3 cells with the mutant plasmids and the IFN-β luciferase construct and then stimulating them with poly(I:C) (Supplemental Figure 7B). Transfection with the S186L allele resulted in the induction of

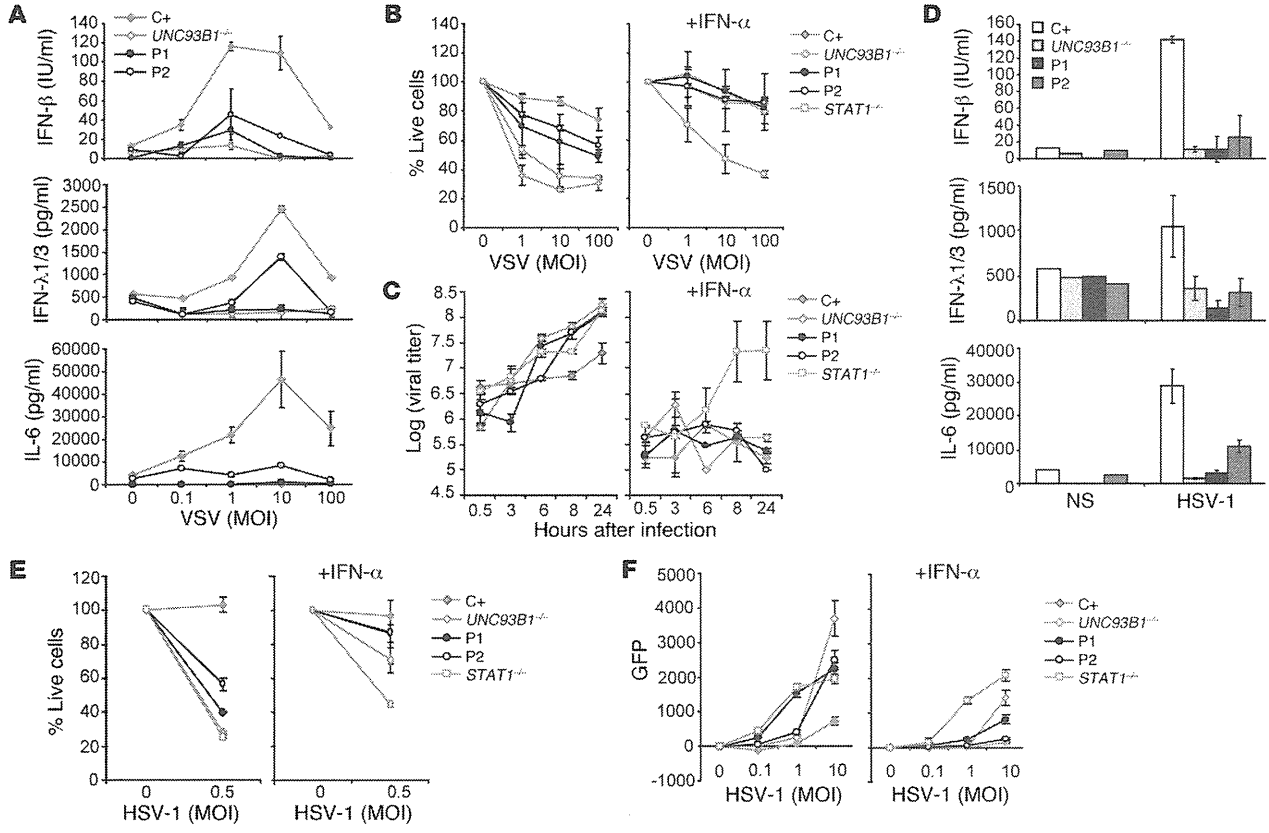

Figure 4

Response to viral infections. (**A**) IFN-β, IFN-λ1/3, and IL-6 production in SV40 fibroblasts 24 hours after infection with VSV. Values (mean ± SEM) were calculated from 3 independent experiments. (**B**) Cell viability of SV40 fibroblasts after 24 hours of infection with VSV in the absence (left) or presence (right) of recombinant IFN-α. The percentage of surviving cells was assessed using resazurin. C+ is a healthy control; *UNC93B1*$^{-/-}$ and *STAT1*$^{-/-}$ cells were used as negative controls. Values (mean ± SEM) were calculated from 3 independent experiments. (**C**) VSV replication in SV40 fibroblasts was estimated at various time points after infection using an MOI of 10. Cells were pretreated with IFN-α or media alone. VSV titer estimation was carried out on Vero cells. Values (mean ± SEM) were calculated from 3 independent experiments. (**D**) IFN-β, IFN-λ1/3, and IL-6 production after infection with 1 MOI of HSV-1 in SV40 fibroblasts after 24 hours. Values (mean ± SEM) were calculated from 3 independent experiments. (**E**) Cell viability of SV40 fibroblasts was assessed using resazurin after 24 hours of HSV-1 infection. C+ is a healthy control; *UNC93B1*$^{-/-}$ and *STAT1*$^{-/-}$ cells were used as negative controls. Cells were pretreated with media (left) or recombinant IFN-α (right). Values (mean ± SEM) were calculated from 3 independent experiments. (**F**) Replication of HSV-1 GFP was assessed in SV40 fibroblasts after 24 hours of infection. Cells were pretreated with media (left) or recombinant IFN-α (right). Values (mean ± SEM) were calculated from 3 independent experiments.

IFN-β upon poly(I:C) stimulation, as observed for the WT TRIF plasmid. After activation by TLR3, TRIF forms homo-oligomers in the cytosol that are responsible for all downstream signaling events (29). These homo-oligomers may be visualized on confocal microscopy as speckle-like structures. Activated TRIF was observed in HeLa cells after poly(I:C) stimulation in cells transfected with the WT or S186L plasmid, suggesting that mutant TRIF was able to interact with TLR3 and homo-oligomerize, like WT TRIF (Supplemental Figure 7C and ref. 29). Data for transient transfection with the S186L allele revealed no difference between the functions of this mutant form and the WT TRIF. The effect of this mutation was undetectable in transient transfection experiments, even if carried out with as little as 10 pg plasmid (data not shown).

Investigating TRIF overexpression in transient transfection. We then addressed the issue of the dominance of the S186L allele. However, as the hypomorphic mutation alone demonstrated normal TRIF function, cotransfection of WT and S186L alleles also revealed normal activation comparable to WT TRIF in 293-TLR3 cells (data not shown). We hypothesize that TRIF levels were already saturated in transient transfection experiments and were therefore not sensitive enough to reveal subtle differences. One of the problems inherent to studies of TRIF overexpression is that the protein is constitutively active and induces apoptosis (20, 33, 34), which does not occur in cells producing small amounts of endogenous TRIF. Indeed, TRIF is normally produced in very small amounts in cells, only transducing and recruiting downstream signaling molecules upon stimulation by TLR3 (29, 35). Thus, the amounts of TRIF protein produced in conditions of overexpression do not reflect physiologically relevant functions of TRIF, as they cause constitutive activation and apoptosis. The transient transfection system has been successfully used by many groups to study the function of TRIF in conditions of overexpression (20, 21, 28, 29,

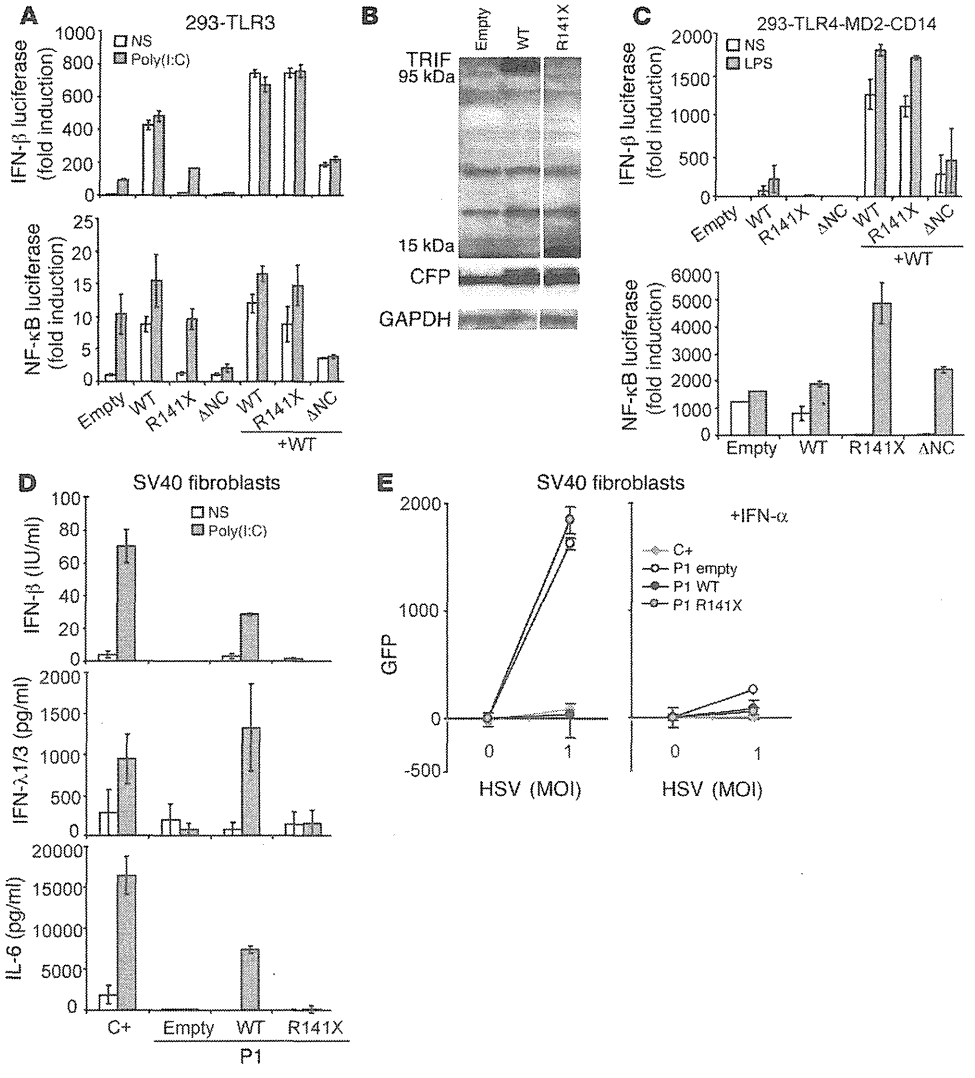

Figure 5

Molecular characterization of the R141X AR TRIF mutation. (**A**) 293 HEK-TLR3 cells were transfected with 10 ng empty vector, WT, R141X, or ΔNC TRIF along with IFN-β–Luc/NF-κB–Luc and RL-TK vectors to assess induction upon overexpression of TRIF. ΔNC TRIF serves as a dominant-negative construct of TRIF, containg only the TIR domain. Transfected cells were left unstimulated or stimulated with 50 μg/ml poly(I:C) for 4 hours. Firefly luciferase values were normalized using renilla values. Total transfected DNA was held constant by adding empty vector. Values (mean ± SEM) were calculated from 3 independent experiments. (**B**) Immunoblot analysis of protein lysates from 293HEK-TLR3–transfected cells, using an antibody recognizing the N-terminal of TRIF. CFP was cotransfected as a control for transfection efficiency. Samples were migrated on the same blot. (**C**) 293HEK-TLR4-MD2-CD14 cells were transfected with 10 ng TRIF vectors, including WT, R141X, and ΔNC TRIF, and the induction of IFN-β–Luc/NF-κB–Luc was assessed by luciferase. Values (mean ± SEM) were calculated from 3 independent experiments. (**D**) Control (C+) SV40 fibroblasts and P1's fibroblasts retrovirally transduced with empty vector, WT TRIF, or R141X TRIF were stimulated with 25 μg/ml poly(I:C) for 24 hours, and production of cytokines was assessed by ELISA. Values (mean ± SEM) were calculated from 3 independent experiments. (**E**) HSV-1 GFP replication was assessed after 24 hours of infection in control SV40 fibroblasts (C+) and SV40 fibroblasts from P1 retrovirally transduced with empty vector, WT, or R141X TRIF. Cells were pretreated with media (left) or recombinant IFN-α (right).Values (mean ± SEM) were calculated from 3 independent experiments.

33, 36). However, a review of the literature showed that no study has ever demonstrated a hypomorphic effect of a point mutation in the context of this transfection system; only null effects have been characterized. These findings support the notion that subtle effects cannot be studied accurately in the context of overexpression.

Functional characterization of the S186L allele in retroviral transduced fibroblasts. We then made use of the fibroblasts available from the patient with AR TRIF deficiency (P1) for retroviral transfection experiments with the S186L allele. Retroviral transduction yielded much lower TRIF levels, although these levels were nonetheless higher than endogenous levels (Supplemental Figure 6). The lack of constitutive activation in retrovirally transduced cells (Figure 5D and Figure 6, B and C) and the low levels of apoptosis suggest that TRIF levels in this system were similar to endogenous levels. They may, therefore, provide ideal conditions for the detection of subtle mutations. The S186L-transduced cells (P1+S186L cells) resulted in significantly lower levels of cytokine production in response to poly(I:C) stimulation compared with P1+WT cells ($P < 0.05$ for all comparisons), suggesting that the S186L allele is hypomorphic (Figure 6B and Supplemental Figure 6A). Furthermore, complementation of fibroblasts from P2, which express endogenous *TRIF*, was achieved with the WT TRIF allele (P2+WT), whereas the S186L allele (P2+S186L) showed impaired responses in terms of the production of IFN-β, IFN-λ, and IL-6 compared with P2+WT cells ($P < 0.05$ for all comparisons) (Figure 6C and Supplemental Figure 6B). Moreover, viral replication after HSV-1 infection in P1+WT cells was comparable to that of a control, whereas P1+S186L cells had significantly higher viral titers compared with those of a control or with P1+WT cells ($P < 0.05$ for both comparisons). There was lower replication in P1+S186L cells than in cells from P1 retrovirally transduced with empty vector (P1+Empty cells) ($P < 0.05$), consistent with a hypomorphic effect (Figure 6D).

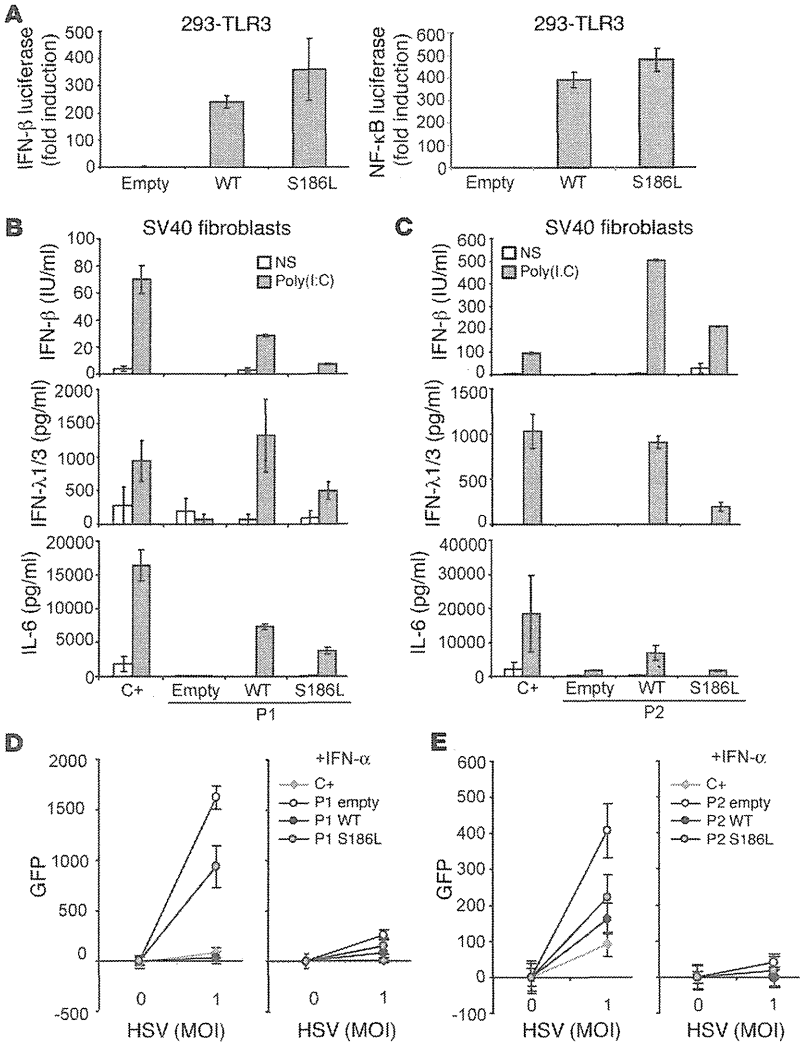

Figure 6
Functional characterization of the S186L AD TRIF mutation. (**A**) 293HEK-TLR3 cells were transfected with empty vector, WT, or S186L TRIF plasmids along with IFN-β–Luc/NF-κB–Luc and RL-TK vectors to assess IFN-β and NF-κB promoter induction upon overexpression of TRIF. Values (mean ± SEM) were calculated from at least 3 independent experiments. (**B**) SV40 fibroblasts from control (C+) and P1's fibroblasts retrovirally transduced with either empty vector, WT TRIF, or S186L TRIF were stimulated with 25 μg/ml poly(I:C) for 24 hours, and the production of cytokines was assessed by ELISA. Values (mean ± SEM) were calculated from at least 3 independent experiments. (**C**) SV40 fibroblasts from control (C+) and P2's fibroblasts retrovirally transduced with empty vector, WT TRIF, or S186L TRIF were stimulated with 25 μg/ml poly(I:C) for 24 hours, and the production of cytokines was assessed by ELISA. Values (mean ± SEM) were calculated from at least 3 independent experiments. (**D**) Replication of HSV-1 GFP was assessed after 24 hours of infection in control SV40 fibroblasts (C+); SV40 fibroblasts from P1 retrovirally transduced with empty vector, WT, or S186L TRIF; and (**E**) SV40 fibroblasts from P2 retrovirally transduced with empty vector, WT, or S186L. Cells were pretreated with media (left) or recombinant IFN-α (right). Values (mean ± SEM) were calculated from at least 3 independent experiments.

Increased HSV-1 replication observed in P2+Empty cells was also complemented in P2+WT cells ($P < 0.05$) (Figure 6E). P2+S186L cells showed a trend toward higher HSV-1 titers compared with that of P2+WT cells, although the difference was not statistically significant, which can be attributed to the hypomorphic nature of the S186L allele. Overall, these data suggest that the S186L mutation is hypomorphic, affecting both the IRF3/IFN-β and NF-κB/IL-6 pathways and controlling susceptibility to HSV-1 infection.

A heterozygous nondeleterious TRIF missense mutation in P3. We identified a third distinct heterozygous mutation in *TRIF* in a boy of Iranian origin (P3), who was born to nonconsanguineous parents and who suffered from HSE at 4.5 years of age (Supplemental Figure 8A). The patient is now 7 years old and has not suffered from other unusual or severe infections. Mutations in the coding regions of *UNC93B1*, *TLR3*, and *TRAF3* were excluded. Further sequencing of leukocyte gDNA from P3 lead to the discovery of a heterozygous missense mutation in TRIF at nucleotide position 1875 (c.1875C>T), resulting in a leucine at amino acid residue 625 in place of a proline in the proline-rich domain of the C terminus of TRIF (P625L) (Supplemental Figure 8, B and C). This mutation was inherited from P3's father who is seronegative for anti–HSV-1 antibodies; hence, P3 remains the only family member affected by HSE. This mutation was not found in the NCBI database, the 1,050 unrelated healthy controls from the CEPH-HGD panel, or in an additional 109 healthy Iranian controls tested, confirming that c.1875C>T is a not a polymorphism. Proline at position 625 was conserved in 7 out of the 11 animal species in which TRIF shares over 50% homology with human TRIF (Supplemental Figure 8D). TRIF protein and mRNA expression were normal in EBV-B cells from P3 (Supplemental Figure 8E and data not shown). This mutation occurred in the proline-rich C-terminal region, implicated in homo-oligomerization, RIP1 binding, NF-κB activation, and apoptosis-inducing functions of TRIF (29, 33). However, despite a poly(I:C) nonresponsive fibroblast phenotype (Supplemental Figure 8F), we did not observe complementation of the phenotype by retroviral transduction of the WT TRIF allele in P3's cells (Supplemental Figure 8H). Moreover, P3's mutation P625L transduced into P1's cells did not differ from WT TRIF–transduced cells in its ability to induce cytokines after poly(I:C) stimulation (Supplemental Figure 8F and Supplemental Figure 6A). Hence, although not found in healthy controls, we were unable to show that this particular mutation is deleterious with the assays available. We hypoth-

esize that P3 carries a pathogenic mutation affecting another gene in the TLR3 signaling pathway. These data neatly illustrate the importance of careful functional characterization of rare mutant alleles, as shown for P2, to ascribe disease responsibility.

Discussion

We report here the first 2 kindreds with AR and AD TRIF deficiencies conferring a predisposition to childhood HSE to our knowledge. The loss-of-expression, loss-of-function, nonsense R141X allele results in the abolition of TLR3-mediated signaling and TRIF-dependent TLR4 responses in the cells of P1. Most family members of P1 are heterozygous carriers of this mutation but have not suffered from HSE or any other infection otherwise. Despite diminished TRIF protein in cells from heterozygous individuals, their leukocytes responded to LPS by the induction of IFN-β transcripts, suggesting that TRIF function was maintained. Moreover, the R141X allele was not dominant negative in 293-TLR3 transfection assays. We did not have access to heterozygous fibroblasts for further testing of the TLR3 pathway, but these results suggest that this defect is purely recessive and that there is no cellular or clinical haploinsufficiency at the *TRIF* locus. The TLR4-TRIF pathway was the only TIR pathway for which no inborn defect had been detected, as it is not defective in patients with UNC-93B, TLR3, MYD88, and IRAK4 deficiencies (10, 11, 13, 37–40). The amounts of IFN-α/β produced in response to the human TRIF-dependent TLR4 pathway are modest, and the role of this pathway in host defense has remained elusive (41, 42). The identification of complete TRIF deficiency in P1, who did not suffer from any infection other than HSE, opportunistic or otherwise, suggests that the human TLR4-TRIF pathway is largely redundant in host defense. Moreover, our study suggests that the recently described role of TRIF in DExD/H-box helicases-dependent cytosolic pathways is also probably redundant for protective immunity (27).

We also identified a patient, P2, with a heterozygous missense mutation in the N-terminal region of TRIF (S186L), defining AD TRIF deficiency as a genetic etiology of HSE. Cells from P2 displayed impaired TLR3-mediated signaling but the maintenance of TRIF-dependent TLR4 responses. The mutant allele showed complete penetrance at the cellular level, because fibroblasts from the 2 TRIF heterozygotes tested, P2 and her mother, showed impaired TLR3 responses. The N-terminal region of TRIF, including the TBK1-binding domain, is indispensable for the IRF3 pathway, consistent with the cellular phenotype of P2, in which IFN-β production and IRF3 dimerization were more affected than the production of IL-6 and NF-κB nuclear translocation after poly(I:C) stimulation (21, 25, 36). P2 fibroblasts were rescued by the WT – but not the mutant TRIF – allele, indicating that the allele is deleterious. The S186L allele appeared functional when used for the transient transfection of 293-TLR3 cells, whereas it was dysfunctional when introduced by retroviral transduction into TRIF-deficient fibroblasts from P1, suggesting that it is hypomorphic but not a complete loss-of-function allele. Data for the kindred with AR complete TRIF deficiency suggest that there is no haploinsufficiency at the *TRIF* locus, pointing toward the notion of the S186L mutation being dominant negative. However, it was difficult to determine experimentally whether the S186L allele was actually dominant negative, as overexpressed TRIF is constitutively active and a potent inducer of apoptosis, preventing fine analysis of the TLR3 pathway. Nonetheless, the available data suggest that the hypomorphic S186L allele of TRIF is probably dominant negative and responsible for AD TRIF deficiency and HSE.

The clinical penetrance of AR TRIF deficiency appears, so far, to be complete, as only one patient with this deficiency has been identified and has had HSE. Similarly, the only known patients with AR TLR3 or AD TRAF3 deficiency also show complete clinical penetrance (12, 13). In contrast, the penetrance of AD TRIF deficiency is incomplete, as only 1 out of the 3 S186L TRIF heterozygotes developed HSE upon infection with HSV-1. This is consistent with AR UNC-93B and AD TLR3 deficiencies, which also show incomplete clinical penetrance (10, 11). Whole-exome sequencing carried out in P2 failed to identify overt deleterious mutations that may explain the variable penetrance (data not shown). In patients with mutations in any of these 4 genes, HSE probably resulted from the impairment of antiviral IFN production in the CNS, leading to higher levels of viral replication and the death of resident cells. The fibroblastic and clinical phenotypes of AR and AD TRIF deficiencies are strikingly similar to those of UNC-93B deficiency (10), TLR3 deficiency (11, 13), and TRAF3 deficiency (12), consistent with the known role of TRIF as the sole adaptor for TLR3. This identification of a fourth gene underlying susceptibility to HSE in 2 kindreds is consistent with our model for the genetic architecture of infectious diseases (18, 43). We proposed that life-threatening pediatric infectious diseases can result from the inheritance of rare single gene mutations, highly deleterious at the cellular level but of variable clinical penetrance (18, 44). Although unlikely, the lack of infectious phenotype or the selective susceptibility to HSE observed in known patients with inborn errors of TLR3 immunity might result from compensatory variations at other loci. The TLR3 pathway is vital for protection against HSE, at least in some children, which may additionally ensure that chronic latency of HSV-1 heightens immunity against other microbes, as shown in the mouse model (45). In any case, HSE provides proof of principle that a collection of single-gene variations displaying incomplete penetrance at the clinical level and affecting different but immunologically related genes may account for severe, sporadic, and common infectious diseases of childhood.

Methods

Patients

We investigated 3 unrelated patients who suffered from HSE during childhood. P1 is a Saudi Arabian boy of consanguineous parents (first cousins). There is no family history of encephalitis, and there was no remarkable infectious history until P1 developed viral meningitis of unknown origin at 1.5 years of age. At the age of 2, he developed HSE, presenting with irritability, fever, and partial seizure. HSE was confirmed by a positive PCR for HSV-1 in the CSF. An MRI scan showed atrophy of the left temporal lobe, and an EEC revealed epileptogenic activity. He suffers from neurological sequelae, mainly consisting of delayed speech. He also has recurrent herpetic stomatitis. He has not yet been exposed to other herpes viruses, determined by negative serology for CMV and VZV.

P2 is a French, Swiss, and Portuguese girl, of nonconsanguineous parents. There is no family history of encephalitis. The mother suffered from meningitis of unknown origin at the age of 9, from which she fully recovered. The mother and maternal grandmother have had herpes labialis. The mother, the maternal grandfather, and P2 are all seropositive for HSV-1. Of note, P2 had a rectovaginal fistula surgical intervention at birth. There was no remarkable infectious history until P2 suffered from serologically determined HSE at 21 months, presenting with high fever. HSE was confirmed

by a positive PCR for HSV-1 in the CSF. Serum analysis detected recent HSV-1 seroconversion. Treatment with acyclovir was administered 4 days after symptoms of fever, after which the patient was hospitalized for treatment. There was no relapse, and she has never suffered from herpes labialis. She suffers from neurological sequelae, mainly consisting of blindness and epilepsy. Following HSE, she has been exposed to other herpes viruses, as shown by positive serology for VZV and EBV with no complications. She has been vaccinated with MMR with no adverse effects.

P3 is an Iranian boy of nonconsanguineous parents. P3 presented with fever, vomiting, and convulsions, with right temporal involvement as shown by MRI. HSE diagnosis was confirmed by an HSV-1–positive PCR in the CSF. Treatment was initiated with acyclovir with no significant improvement. Subsequent treatment with foscarnet for 21 days was successful. At day 23, symptoms of low consciousness and choreatic movement were observed along with a positive PCR for HSV-1. Treatment with cidofovir was administered for 5 days, and he has fully recovered. P3 has not yet been exposed to other herpes viruses, such as VZV and EBV, as determined by negative serology. Of note, the father who carries the mutation is seronegative for serum antibodies to HSV, whereas the mother is seropositive. There is no remarkable medical history in the family.

Cell lines

Skin biopsy specimens from the patients as well as family members, the UNC-93B–deficient patient, TLR3-deficient patient, the MyD88-deficient patient, the STAT1-deficient patient, and healthy controls were obtained for the establishment of primary fibroblasts. Primary fibroblasts were cultured in DMEM supplemented with 10% FBS, 10 U/ml penicillin, 10 μg/ml streptomycin, and 62.5 ng/ml amphotericin B (Invitrogen). Fibroblasts were immortalized with the SV40 large T antigen, as previously described (46). NEMO-deficient immortalized fibroblasts were derived from a fetus with incontinentia pigmenti (47). All cell lines were incubated at 37°C, under an atmosphere containing 5% CO_2. PBMCs from patients and healthy controls were harvested from fresh blood by Ficoll-Hypaque density gradient centrifugation (GE Healthcare). PBMCs were cultured in RPMI supplemented with 10% FBS (Invitrogen) or 1% human sera.

Activation by TLR ligands

A synthetic analog of dsRNA, poly(I:C) (TLR3 agonist, at 25 μg/ml), and LPS (LPS *Salmonella minnesota*, TLR-4 agonist, at 10 to 100 ng/ml) were purchased from Invivogen; resiquimod hydrochloride (R-848; TLR-7, and TLR-8 agonist, at 3 μg/ml) was purchased from GLSynthesis Inc.; unmethylated CpG DNA CpG-A (D19) (TLR-9 agonist, at 5 μg/ml) was provided by Robert Coffman and Frank Barrat (both from Dynavax Technologies, Berkeley, California); and IL-1β (at 20 ng/ml) and TNF-α (at 20 ng/ml) were obtained from R&D Systems. All agonists and reagents were endotoxin free. In all stimulations of PBMCs with TLR agonists other than LPS, the cells were incubated with 10 μg/ml polymyxin B (Sigma-Aldrich), at 37°C, for 30 minutes before activation. TLR agonists were used to stimulate PBMCs for 48 hours, at a concentration of 2×10^6 cells per ml in RPMI 1640 supplemented with 10% FBS or 1% human serum. The SV40-fibroblast cell lines were activated in 24-well plates, at a density of 10^5 cells per well, for 24 hours with poly(I:C) (25 μg/ml), TNF-α (20 ng/ml), IL-1β (20 ng/ml), IPH 3102 or poly(A:U) (50 μg/ml) TLR3-specific ligand (Innate Pharma), and 7sk-as (provided by Caetano Reis e Sousa, London Research Institute, London, United Kingdom).

Viral infections for cytokine determination

PBMCs isolated by Ficoll-Paque density gradient centrifugation were stimulated with various intact viruses for 24 hours, at a density of 2×10^6 cells per ml in RPMI 1640 supplemented with 10% FBS or, for some experiments, 2% FBS. The following viruses were used: the dsDNA virus HSV-1 (KOS-1 strain, MOI = 1) and the ss(–)RNA virus VSV (Indiana strain, MOI = 1). The SV40-fibroblast cell lines were activated in 24-well plates, at a density of 10^5 cells per well, for 24 hours with HSV-1 or VSV. Cell supernatants were recovered and tested for cytokine production by ELISA.

Cytokine determinations

The production of IFN-α, IFN-β, IFN-λ1/3, and IL-6 was assessed by ELISA, according to the kit manufacturer's instructions, respectively: Human IFN-α Module Set (AbCys SA), Human IFN-β ELISA Kit (TFB, Fujirebio Inc.), Duo Set Human IL29/IL28B (IFN-λ1/3) (R&D Systems), and Human IL-6 (Sanquin).

Q-PCR

Total RNA was extracted from cells either unstimulated or stimulated with TLR agonists. All RNA samples were treated with RNase-free DNase (Qiagen) after isolation with the RNeasy Extraction Kit (Qiagen). RNA was reverse transcribed directly, with the High Capacity RNA-to-cDNA Master Mix (Applied Biosystems). Q-PCR was performed with Applied Biosystems Assays-on-Demand probe/primer combinations specific for IFN-β, IL-6, TRIF, and β-glucuronidase (GUS), which was used for normalization. Results are expressed according to the ΔΔCt method, as described by the manufacturer.

Western blots

Total cell extracts were prepared from 293-NULL, 293-TLR3, 293-TLR4-MD2-CD14, SV40 fibroblasts, and EBV-B cells. Equal amounts of protein from each sample were separated on SDS-PAGE gels and blotted onto iBLOT gel transfer stacks (Invitrogen), which were then probed with antibodies and developed with peroxidase-conjugated secondary antibodies and ECL Western blotting substrate (GE Healthcare). TRIF antibodies binding to the N-terminal region of human TRIF (Alexis Biochemicals) were used for Western blots. Anti-CFP (Abcam), anti-ACTIN, anti-GAPDH (Santa Cruz Biotechnology Inc.), and anti-HA antibodies (Sigma-Aldrich) were also used.

Signal transduction studies

Nuclear cell extracts were prepared from SV40-fibroblasts after incubation with or without poly(I:C), TNF-α, and IL-1β. TransAM NF-κB p65 ELISA (Active Motif) was performed with an NF-κB p65-specific DNA probe and 10 μg nuclear extract. The Bio-Rad protein assay was used to determine protein concentrations. For the detection of IRF3 dimerization, whole-cell extracts were prepared from SV40-fibroblasts with or without poly(I:C) treatment. The IRF3 monomers and dimers were separated by native PAGE in the presence of 1% sodium deoxycholate (DOC) (Sigma-Aldrich). Total cell extracts (25 μg of protein) were diluted 1:2 in nondenaturing sample buffer (125 mM Tris-HCl, pH 6.8, 30% glycerol, and 2% DOC) and separated by electrophoresis in a 7.5% polyacrylamide gel, in 25 mM Tris and 192 mM glycine, pH 8.4, with 1% DOC present in the cathode chamber only. The gel was blotted onto a membrane, which was then probed with the anti-IRF3 antibody (FL-425, Santa Cruz Biotechnology Inc.).

Transient transfections and reporter assays

The mutant alleles were generated with the QuikChange II Site-Directed Mutagenesis Kit from Qiagen for introduction of the C421T, C557T, and C1875T mutations into the pEF-Bos-TRIF plasmid C-terminally tagged with HA (provided by Misako Matsumoto). The pcDNA3-CFP vector (Addgene) was used to control for transfection efficiency. The ΔNC TRIF construct was a gift from Osamu Takeuchi (Osaka University, Osaka, Japan). pGL4.32[*luc2P*/NF-κB-RE/Hygro] NF-κB luciferase and pRL-TK *Renilla*

luciferase plasmids were purchased from Promega Corporation. The IFN-β promoter-luciferase construct was provided by Christopher Basler (Mount Sinai School of Medicine, New York, New York, USA). 293-NULL, 293-hTLR3, or 293-hTLR4A-MD2-CD14 cells (Invivogen) were plated in 24-well plates and transfected with the expression vectors in the presence of lipofectamine LTX reagent, according to the manufacturer's instructions (Invitrogen). The total amount of DNA was kept constant with empty vector (1 μg/well). Apoptosis was inhibited by adding 20 μM z-VAD-fmk (Sigma-Aldrich) to each well. Twenty hours after transfection, the cells were incubated for 4 hours more, with or without 50 μg/ml poly(I:C). Cell lysates were obtained and analyzed with the Dual-Luciferase Reporter Assay System (Promega Corporation), according to the manufacturer's instructions. Firefly luciferase values were normalized against *Renilla* luciferase activity and expressed as fold change with respect to cells transfected with the empty vector.

Confocal microscopy

HeLa cells were transfected with the expression plasmid for WT TICAM-1 (WT) or the S186L mutant (0.2 ng); 24 hours after transfection, cells were stimulated with buffer alone or with 10 μg/ml poly(I:C) for 30 minutes. Cells were fixed in 4% paraformaldehyde for 30 minutes and permeabilized with 0.2% Triton X-100 in PBS for 10 minutes. Fixed cells were blocked in 1% bovine serum albumin in PBS and labeled by incubation with anti-HA pAb for 60 minutes at room temperature. Alexa Fluor 594–conjugated secondary antibodies (1:400) were used to visualize the primary antibody. Nuclei were stained with DAPI (2 μg/ml) in PBS for 10 minutes, before being mounted on glass slides in PBS supplemented with 2.3% 1,4-diazabicyclo[2.2.2]octane and 50% glycerol. Cells were visualized at ×63 magnification, with an LSM510 META microscope (Zeiss).

Retroviral transduction of SV40 fibroblasts

The doxycycline-inducible expression plasmid (pLINX-Flag) and pLINX-Flag-TRIF were provided by Sang Hoon Rhee (UCLA, Los Angeles, California, USA). The C421T, C557T, and C1875T mutations were introduced into the pLINX-Flag-TRIF plasmid by site-directed mutagenesis, as described above. 293T cells (ATCC no. CRL-11268) were grown in DMEM (Gibco BRL/Invitrogen) supplemented with 10% heat-inactivated FBS, 50 IU/ml penicillin, and 50 μg/ml streptomycin (Gibco BRL/Invitrogen) at 37°C in a humidified atmosphere containing 5% CO_2. Retroviral vectors pseudotyped with the vesicular stomatitis G protein (VSV-G) were generated as previously described (48) by calcium phosphate transfection into 293T cells of a packaging construct, pMNold gag-pol; a plasmid producing the VSV-G envelope (pMD.G); and each of the pLINX vectors. Culture medium was collected at 24, 48, and 72 hours, pooled, 0.45-μ filtered, and concentrated approximately 1,000 fold by ultracentrifugation. Fibroblasts (1.5×10^5 cells per well) were seeded into a 12-well dish and infected on the following day, with 8 to 16 μl of each retroviral vector for 4 hours. Twenty-four hours later, the medium was replaced with DMEM containing 1 μg/ml doxycycline (Clonetech) to prevent expression of the TRIF cDNA insert. Forty-eight hours later, DMEM containing doxycycline and 1 mg/ml G418 (Invivogen) was added to the cells. Selected cells were amplified. The stably transduced cells were then plated in 24-well plates without doxycycline for 24 hours and stimulated with 25 μg/ml poly(I:C) for an additional 24 hours. The cells were lysed after 48 hours of culture in the absence of doxycycline.

Viral replication

For viral titration of VSV, 10^5 SV40-fibroblasts were plated in each well of a 24-well plate and infected at a MOI of 10 in DMEM supplemented with 2% FBS. The Stat-1–deficient patient has been described elsewhere (46). After 30 minutes, cells were washed and incubated in 500 μl of medium. All cells and supernatants were harvested and frozen at the time points indicated in the figures. Viral titers were determined by calculating the 50% end point ($TCID_{50}$), as described by Reed and Muench, after the inoculation of Vero cell cultures in 96-well plates. For HSV-1 replication, HSV-1 GFP (strain KOS) (49), at MOIs ranging from 0.1–10, was used to infect the 10^4 SV40 fibroblasts plated in 96-well plates. The GFP fluorescence of the samples was quantified after 24 hours. For assays of cell protection upon viral stimulation, cells were treated with IFN-α2b (Schering-Plough, 1×10^5 IU/ml) 18 hours before infection and during infection.

Cell viability assay

The viability of SV40-fibroblasts was assessed by resazurin oxidoreduction (TOX-8) (Sigma-Aldrich). Cells were plated in triplicate in 96-well flat-bottomed plates (2×10^4 cells/well) in DMEM supplemented with 2% FBS. Cells were infected with VSV or HSV-1 for 24 hours at the indicated MOI. Resazurin dye solution was then added, and the samples were incubated for an additional 2 hours at 37°C. Fluorescence was then measured at a wavelength of 590/560 nm. Background fluorescence, calculated for dye and complete medium alone (in the absence of cells), was then subtracted from the values for all the other samples; 100% viability corresponds to the fluorescence of uninfected cells. For assays of cell protection upon viral stimulation, cells were treated with IFN-α2b (Schering-Plough, 1×10^5 IU/ml) for 18 hours before infection and during infection.

Genome-wide transcriptional profile studies in fibroblasts and PBMCs

Microarray. SV40 fibroblasts obtained from patients or control subjects were stimulated with 25 μg/ml poly(I:C) or 20 ng/ml IL-1β or left unstimulated for 4 hours. Previously frozen PBMCs from patients or control subjects were left overnight in 10% FBS RPMI and then stimulated with 10 ng/ml LPS or 3 μg/ml R848 or left unstimulated for 2 hours. Total RNA was isolated (RNeasy Kit, Qiagen), and RNA integrity was assessed on an Agilent 2100 Bioanalyzer (Agilent). Biotinylated cRNA targets were prepared from 100 to 250 ng total RNA, using the Illumina TotalPrep RNA Amplification Kit (Ambion). The labelled cRNA (750 ng) were then incubated for 16 hours to HT-12 v4 BeadArrays (48,323 probes). Beadchip arrays were then washed, stained, and scanned on an Illumina HiScanSQ according to the manufacturer's instructions.

Data preprocessing. For the analysis of SV40 fibroblasts and PBMCs, after background subtraction, the raw signal values extracted with Illumina Beadstudio (version 2) were scaled using quantile normalization. Minimum intensity was set to 10, and all the intensity values were $\log_2$ transformed. Only the probes called present in at least 1 sample ($P < 0.01$) were retained for downstream analysis ($n = 23{,}281$ and $n = 22{,}881$ for fibroblasts and PBMCs, respectively).

Data analysis. Transcripts differentially regulated upon stimulation were defined based on a minimum 2-fold change (upregulation or downregulation) and a minimum absolute raw intensity difference of 100 with respect to the respective unstimulated sample. Heat maps were generated using R (version 2.12.2). Raw data from this study are available in the Gene Expression Omnibus repository (accession no. GSE32390; http://www.ncbi.nlm.nih.gov/gds).

DNA samples

Control gDNA samples were obtained from the CEPH for the 1,052 individuals from the CEPH-HGD panel. An additional 182 genomic samples were obtained from Prince Naif Center for Immunology Research, King Khalid University Hospital (KKUH), Riyadh, Saudi Arabia, for a panel of control Saudi Arabian children aged between 6 and 8 years old. This study was approved by the College of Medicine Research Council (CMRC) Ethical

Committee of the KKUH. Informed written consent was obtained from the patients' parents or guardians. The male-to-female ratio was approximately 2:1. In order to validate the P625L variant in a control Iranian population, we used 109 gDNA samples collected from healthy blood donors referred to the Medical Laboratories of the Arad General Hospital in Tehran. All individuals were from both sexes, from Tehran, and represent different ethnic groups, which are considered to be representative of the general Iranian population. DNA was extracted from whole blood. All data and the collection of samples were approved by the Iranian National Ethics Committee.

Statistics

Unless otherwise specified, mean values ± SEM were calculated for all results. The Student's *t* test (2 tailed) was used to determine significance, where $P < 0.05$ was found to be statistically significant.

Study approval

The experiments described here were conducted in France in accordance with local regulations approved by the CMRC Ethical Committee of the KKUH, the IRB of Necker Enfants Malades Hospital, and the IRB of Mofid Children Hospital.

Acknowledgments

We thank the members of the Laboratory of Human Genetics of Infectious Diseases, in particular Mélanie Migaud, Isabelle Melki, Martine Courat, Tony Leclerc, and Yelena Nemirovskaya; M. Oritz Lombardo for helpful discussions and technical assistance; Osamu Takeuchi for the dominant-negative TRIF vector; Sang Hoon Rhee for the doxycycline-inducible TRIF plasmid; Christopher Basler for the IFNB-luciferase plasmid; and Marianne Leruez for viral serology. We thank the children and their families for participating in this study. V. Sancho-Shimizu was supported by the Marie Curie Intra-European Fellowship 2008-2010. J.-L. Casanova was an international scholar of the Howard Hughes Medical Institute from 2005 to 2008. The Laboratory of Human Genetics of Infectious Diseases is supported by grants from the Agence national de la Recherche (ANR-08-MNP-014), The Rockefeller University Center for Clinical and Translational Science (grant no. 5UL1RR024143-03), and The Rockefeller University.

Received for publication May 31, 2011, and accepted in revised form October 6, 2011.

Address correspondence to: Vanessa Sancho-Shimizu, Faculty of Medicine Necker Hospital, 156 rue Vaugirard, 75015 Paris. Phone: 33.1.40.61.55.39; Fax: 33.1.40.61.56.88; E-mail: vanessa.sancho-shimizu@inserm.fr. Or to: Jean-Laurent Casanova, The Rockefeller University, 1230 York Avenue, New York, New York 10065, USA. Phone: 212.327.7331; Fax: 212.327.7330; E-mail: casanova@rockefeller.edu.

1. Whitley RJ. Herpes simplex virus in children. *Curr Treat Options Neurol.* 2002;4(3):231–237.
2. Whitley RJ, et al. Vidarabine versus acyclovir therapy in herpes simplex encephalitis. *N Engl J Med.* 1986;314(3):144–149.
3. Whitley RJ, Lakeman F. Herpes simplex virus infections of the central nervous system: therapeutic and diagnostic considerations. *Clin Infect Dis.* 1995; 20(2):414–420.
4. McGrath N, Anderson NE, Croxson MC, Powell KF. Herpes simplex encephalitis treated with acyclovir: diagnosis and long term outcome. *J Neurol Neurosurg Psychiatry.* 1997;63(3):321–326.
5. Gordon B, Selnes OA, Hart J Jr, Hanley DF, Whitley RJ. Long-term cognitive sequelae of acyclovir-treated herpes simplex encephalitis. *Arch Neurol.* 1990;47(6):646–647.
6. Sancho-Shimizu V, et al. Genetic susceptibility to herpes simplex virus 1 encephalitis in mice and humans. *Curr Opin Allergy Clin Immunol.* 2007;7(6):495–505.
7. Whitley RJ, Gnann JW. Viral encephalitis: familiar infections and emerging pathogens. *Lancet.* 2002;359(9305):507–513.
8. Abel L, et al. Age-dependent Mendelian predisposition to herpes simplex virus type 1 encephalitis in childhood. *J Pediatr.* 2010;157(4):623–629.
9. De Tiege X, Rozenberg F, Heron B. The spectrum of herpes simplex encephalitis in children. *Eur J Paediatr Neurol.* 2008;12(2):72–81.
10. Casrouge A, et al. Herpes simplex virus encephalitis in human UNC-93B deficiency. *Science.* 2006; 314(5797):308–312.
11. Zhang SY, et al. TLR3 deficiency in patients with herpes simplex encephalitis. *Science.* 2007; 317(5844):1522–1527.
12. Perez de Diego R, et al. Human TRAF3 adaptor molecule deficiency leads to impaired Toll-like receptor 3 response and susceptibility to herpes simplex encephalitis. *Immunity.* 2010;33(3):400–411.
13. Guo Y, et al. Herpes simplex virus encephalitis in a patient with complete TLR3 deficiency: TLR3 is otherwise redundant in protective immunity. *J Exp Med.* 2011;208(10):2083–2098.
14. Dupuis S, et al. Impaired response to interferon-alpha/beta and lethal viral disease in human STAT1 deficiency. *Nat Genet.* 2003;33(3):388–391.
15. Audry M, et al. NEMO is a key component of NF-κB- and IRF-3-dependent TLR3-mediated immunity to herpes simplex virus. *J Allergy Clin Immunol.* 2011;128(3):610–617.
16. Jouanguy E, et al. Human primary immunodeficiencies of type I interferons. *Biochimie.* 2007; 89(6-7):878–883.
17. Zhang SY, et al. Human Toll-like receptor-dependent induction of interferons in protective immunity to viruses. *Immunol Rev.* 2007;220:225–236.
18. Alcaïs A, Quintana-Murci L, Thaler DS, Schurr E, Abel L, Casanova JL. Life-threatening infectious diseases of childhood: single-gene inborn errors of immunity? *Ann N Y Acad Sci.* 2010;1214:18–33.
19. Matsumoto M, Kikkawa S, Kohase M, Miyake K, Seya T. Establishment of a monoclonal antibody against human Toll-like receptor 3 that blocks double-stranded RNA-mediated signaling. *Biochem Biophys Res Commun.* 2002;293(5):1364–1369.
20. Yamamoto M, et al. Cutting edge: a novel Toll/IL-1 receptor domain-containing adapter that preferentially activates the IFN-beta promoter in the Toll-like receptor signaling. *J Immunol.* 2002; 169(12):6668–6672.
21. Oshiumi H, Matsumoto M, Funami K, Akazawa T, Seya T. TICAM-1, an adaptor molecule that participates in Toll-like receptor 3-mediated interferon-beta induction. *Nat Immunol.* 2003;4(2):161–167.
22. Fitzgerald KA, et al. LPS-TLR4 signaling to IRF-3/7 and NF-kappaB involves the toll adapters TRAM and TRIF. *J Exp Med.* 2003;198(7):1043–1055.
23. Oshiumi H, et al. TIR-containing adapter molecule (TICAM)-2, a bridging adapter recruiting to toll-like receptor 4 TICAM-1 that induces interferon-beta. *J Biol Chem.* 2003;278(50):49751–49762.
24. Yamamoto M, et al. TRAM is specifically involved in the Toll-like receptor 4-mediated MyD88-independent signaling pathway. *Nat Immunol.* 2003; 4(11):1144–1150.
25. Yamamoto M, et al. Role of adaptor TRIF in the MyD88-independent toll-like receptor signaling pathway. *Science.* 2003;301(5633):640–643.
26. Hoebe K, et al. Identification of Lps2 as a key transducer of MyD88-independent TIR signalling. *Nature.* 2003;424(6950):743–748.
27. Zhang Z, et al. DDX1, DDX21, and DHX36 helicases form a complex with the adaptor molecule TRIF to sense dsRNA in dendritic cells. *Immunity.* 2011;34(6):866–878.
28. Jiang Z, Mak TW, Sen G, Li X. Toll-like receptor 3-mediated activation of NF-kappaB and IRF3 diverges at Toll-IL-1 receptor domain-containing adapter inducing IFN-beta. *Proc Natl Acad Sci U S A.* 2004;101(10):3533–3538.
29. Funami K, Sasai M, Oshiumi H, Seya T, Matsumoto M. Homo-oligomerization is essential for Toll/interleukin-1 receptor domain-containing adaptor molecule-1-mediated NF-kappaB and interferon regulatory factor-3 activation. *J Biol Chem.* 2008; 283(26):18283–18291.
30. Pichlmair A, et al. RIG-I-mediated antiviral responses to single-stranded RNA bearing 5'-phosphates. *Science.* 2006;314(5801):997–1001.
31. Meylan E, Tschopp J. Toll-like receptors and RNA helicases: two parallel ways to trigger antiviral responses. *Mol Cell.* 2006;22(5):561–569.
32. Yoneyama M, Fujita T. Function of RIG-I-like receptors in antiviral innate immunity. *J Biol Chem.* 2007;282(21):15315–15318.
33. Kaiser WJ, Offermann MK. Apoptosis induced by the toll-like receptor adaptor TRIF is dependent on its receptor interacting protein homotypic interaction motif. *J Immunol.* 2005;174(8):4942–4952.
34. Han KJ, et al. Mechanisms of the TRIF-induced interferon-stimulated response element and NF-kappaB activation and apoptosis pathways. *J Biol Chem.* 2004;279(15):15652–15661.
35. Funami K, et al. Spatiotemporal mobilization of Toll/IL-1 receptor domain-containing adaptor molecule-1 in response to dsRNA. *J Immunol.* 2007; 179(10):6867–6872.
36. Tatematsu M, et al. A molecular mechanism for Toll-IL-1 receptor domain-containing adaptor molecule-1-mediated IRF-3 activation. *J Biol Chem.* 2010; 285(26):20128–20136.
37. von Bernuth H, et al. Pyogenic bacterial infections in humans with MyD88 deficiency. *Science.* 2008;321(5889):691–696.
38. Picard C, et al. Pyogenic bacterial infections in humans with IRAK-4 deficiency. *Science.* 2003; 299(5615):2076–2079.
39. Ku CL, et al. IRAK4 and NEMO mutations in other-

wise healthy children with recurrent invasive pneumococcal disease. *J Med Genet.* 2007;44(1):16–23.
40. Casanova JL, Abel L, Quintana-Murci L. Human TLRs and IL-1Rs in host defense: natural insights from evolutionary, epidemiological, and clinical genetics. *Annu Rev Immunol.* 2011;29:447–491.
41. Yang K, et al. Human TLR-7-, -8-, and -9-mediated induction of IFN-alpha/beta and -lambda is IRAK-4 dependent and redundant for protective immunity to viruses. *Immunity.* 2005;23(5):465–478.
42. Ku CL, et al. Inherited disorders of human Toll-like receptor signaling: immunological implications. *Immunol Rev.* 2005;203:10–20.
43. Alcais A, Abel L, Casanova JL. Human genetics of infectious diseases: between proof of principle and paradigm. *J Clin Invest.* 2009;119(9):2506–2514.
44. Casanova JL, Abel L. Primary immunodeficiencies: a field in its infancy. *Science.* 2007;317(5838):617–619.
45. Barton ES, et al. Herpesvirus latency confers symbiotic protection from bacterial infection. *Nature.* 2007;447(7142):326–329.
46. Chapgier A, et al. Human complete Stat-1 deficiency is associated with defective type I and II IFN responses in vitro but immunity to some low virulence viruses in vivo. *J Immunol.* 2006;176(8):5078–5083.
47. Smahi A, et al. Genomic rearrangement in NEMO impairs NF-kappaB activation and is a cause of incontinentia pigmenti. The International Incontinentia Pigmenti (IP) Consortium. *Nature.* 2000; 405(6785):466–472.
48. Barde I, et al. Efficient control of gene expression in the hematopoietic system using a single Tet-on inducible lentiviral vector. *Mol Ther.* 2006;13(2):382–390.
49. Desai P, Person S. Incorporation of the green fluorescent protein into the herpes simplex virus type 1 capsid. *J Virol.* 1998;72(9):7563–7568.

Published October 12, 2011, doi:10.4049/jimmunol.1101503

The TLR3/TICAM-1 Pathway Is Mandatory for Innate Immune Responses to Poliovirus Infection

Hiroyuki Oshiumi,*,[1] Masaaki Okamoto,*,[1] Ken Fujii,[†] Takashi Kawanishi,* Misako Matsumoto,* Satoshi Koike,[†] and Tsukasa Seya*

Cytoplasmic and endosomal RNA sensors recognize RNA virus infection and signals to protect host cells by inducing type I IFN. The cytoplasmic RNA sensors, retinoic acid inducible gene I/melanoma differentiation-associated gene 5, actually play pivotal roles in sensing virus replication. IFN-β promoter stimulator-1 (IPS-1) is their common adaptor for IFN-inducing signaling. Toll/IL-1R homology domain-containing adaptor molecule 1 (TICAM-1), also known as TRIF, is the adaptor for TLR3 that recognizes viral dsRNA in the early endosome in dendritic cells and macrophages. Poliovirus (PV) belongs to the Picornaviridae, and melanoma differentiation-associated gene 5 reportedly detects replication of picornaviruses, leading to the induction of type I IFN. In this study, we present evidence that the TLR3/TICAM-1 pathway governs IFN induction and host protection against PV infection. Using human PVR transgenic (PVRtg) mice, as well as IPS-$1^{-/-}$ and TICAM-$1^{-/-}$ mice, we found that TICAM-1 is essential for antiviral responses that suppress PV infection. TICAM-$1^{-/-}$ mice in the PVRtg background became markedly susceptible to PV, and their survival rates were decreased compared with wild-type or IPS-$1^{-/-}$ mice. Similarly, serum and organ IFN levels were markedly reduced in TICAM-$1^{-/-}$/PVRtg mice, particularly in the spleen and spinal cord. The sources of type I IFN were $CD8\alpha^{+}$ /$CD11c^{+}$ splenic dendritic cells and macrophages, where the TICAM-1 pathway was more crucial for PV-derived IFN induction than was the IPS-1 pathway in ex vivo and in vitro analyses. These data indicate that the TLR3/TICAM-1 pathway functions are dominant in host protection and innate immune responses against PV infection. ***The Journal of Immunology*, 2011, 187: 000–000.**

When RNA viruses infect mammalian cells, type I IFN is generated to suppress viral infection. IFN-inducing pathways evoked by viral dsRNA have been identified in humans and mice, and the possible involvement of these pathways in protection against viruses has been examined using gene-disrupted mice and various virus species (1). The sensing of dsRNA by the innate immune system is accomplished either by TLR3 or by cytoplasmic sensors such as dsRNA-dependent protein kinase (so-called PKR), retinoic acid inducible gene I (RIG-I), and melanoma differentiation-associated gene 5 (MDA5) (2). In virus-infected cells, RIG-I and MDA5 mainly participate in type I IFN induction in conjunction with the adaptor molecule IFN-β promoter stimulator-1 (IPS-1; also known as MAVS, Cardif, or VISA) (1). The role of these molecules in host cell protection has been clearly delineated in RNA virus infection.

Toll/IL-1R homology domain-containing adaptor molecule 1 (TICAM-1; also called TRIF) is the adaptor of TLR3 (3–5). When TLR3 senses dsRNA on the endosomal membrane, it induces type I IFN (6, 7). The adaptor TICAM-1 plays a pivotal role in TLR3-mediated IFN-α/β induction. Once dsRNA stimulates TLR3, TICAM-1 transiently couples with TLR3 and forms a multimer, translocating to a distinct region of the cytoplasm (8). In its multimeric form, TICAM-1 recruits the kinase complex to activate IFN regulatory factors (IRF)-3 and -7, which induce type I IFN production (7, 9). Historically, this IFN-inducing pathway was identified earlier than the cytoplasmic RIG-I/MDA5 pathway (10, 11). Many reports have mentioned the possibility that the TLR3/TICAM-1 pathway is involved in the anti-viral IFN response (12), but no definitive evidence of the anti-viral properties of this pathway has been obtained using TICAM-$1^{-/-}$ mice (13). Only a DNA virus, mouse CMV (MCMV), has been shown to infect TICAM-$1^{-/-}$ mice, and thus mouse cells are partly protected from MCMV by the TICAM-1 pathway (5, 14).

Poliovirus (PV) is a positive strand ssRNA virus that produces dsRNA intermediates during viral replication (15), modified with 5′ terminal Vpg protein (16), a characteristic feature of picornaviruses. It is generally accepted that picornaviruses are recognized by MDA5 but not RIG-I in infected cells, presumably due to the generation of this unusual dsRNA. This concept was confirmed by the finding that MDA5$^{-/-}$ mice fail to induce type I IFN in response to encephalomyocarditis virus (EMCV) and permit severe EMCV infection (13, 17). However, another picornavirus, coxsackie B virus (CBV) serotype 3, is recognized by TLR3 in infected cells and induces IFN-γ as an effector for suppressing CBV infection

*Department of Microbiology and Immunology, Hokkaido University Graduate School of Medicine, Sapporo 060-8638, Japan; and [†]Department of Microbiology and Immunology, Tokyo Metropolitan Institute for Neuroscience, Tokyo Metropolitan Organization for Medical Research, Tokyo 156-0057, Japan

[1]H.O. and M.O. contributed equally to this work.

Received for publication May 24, 2011. Accepted for publication September 6, 2011.

This work was supported in part by Grants-in-Aid from the Ministry of Education, Science, and Culture of Japan (Specified Project for Advanced Research), the Ministry of Health, Labor, and Welfare of Japan, the Takeda Foundation, and by the Waxmann Foundation. Financial support by the Program of Founding Research Centers for Emerging and Reemerging Infectious Diseases, Ministry of Education, Culture, Sports, Science, and Technology of Japan, is gratefully acknowledged.

Address correspondence and reprint requests to Prof. Tsukasa Seya, Department of Microbiology and Immunology, Graduate School of Medicine, Hokkaido University, Kita-ku, Kita-15 Nishi-17, Sapporo, Hokkaido 060-8638, Japan. E-mail address: seya-tu@pop.med.hokudai.ac.jp

The online version of this article contains supplemental material.

Abbreviations used in this article: BM, bone marrow; BM-DC, bone marrow-derived dendritic cell; BM-Mf, bone marrow-derived macrophage; CBV, coxsackie B virus; DC, dendritic cell; EMCV, encephalomyocarditis virus; HCV, hepatitis C virus; IFIT-1, IFN-induced protein with tetratripeptide repeats 1; IP-10, IFN-γ–induced protein 10; IPS-1, IFN-β promoter stimulator-1; IRF, IFN regulatory factor; KO, knockout; MCMV, mouse cytomegalovirus; MDA5, melanoma differentiation-associated gene 5; MEF, mouse embryonic fibroblast; Mf, macrophage; MOI, multiplicity of infection; PV, poliovirus; PVRtg, poliovirus receptor transgenic; RIG-I, retinoic acid inducible gene I; RT-qPCR, real-time quantitative PCR; TICAM-1, Toll/IL-1R homology domain-containing adaptor molecule 1; WNV, West Nile virus; WT, wild-type.

www.jimmunol.org/cgi/doi/10.4049/jimmunol.1101503

(18). In this study, we analyzed in vivo infection of a popular picornavirus, PV, using PVR transgenic (PVRtg) mice, which show a neurotropic phenotype during PV infection similar to humans (19, 20). Using this mouse model, in combination with TICAM-1$^{-/-}$ or IPS-1$^{-/-}$ mice, we present evidence that the host TICAM-1 pathway, particularly in macrophages (Mf), serves as a source of type I IFN induction and protects host PVRtg mice from PV infection and paralytic death. Thus, the strategy for host protection against picornaviruses is not simply based on the MDA5-dependent dsRNA recognition, but is variable depending on picornavirus species.

Materials and Methods

Mice

All mice were backcrossed with C57BL/6 mice more than seven times before use. TICAM-1$^{-/-}$ (21) and IPS-1$^{-/-}$ mice (this study) were generated in our laboratory. TLR3$^{-/-}$ (4), IRF-3$^{-/-}$, and IRF-7$^{-/-}$ mice (22) were provided by Drs. S. Akira (Osaka University, Osaka, Japan) and T. Taniguchi (University of Tokyo, Tokyo, Japan). PVRtg mice were provided as reported previously (20). All mice were maintained under specific pathogen-free conditions in the Animal Facility at Hokkaido University Graduate School of Medicine (Sapporo, Japan). Animal experiments were performed according to the guidelines set by the Animal Safety Center, Japan.

Generation of IPS-1–deficient mice

The *IPS-1* gene was amplified by PCR using genomic DNA extracted from embryonic stem cells. The targeting vector was constructed by replacing the second and third exons with a neomycin-resistance gene cassette (Neo), and an HSV thymidine kinase driven by the PGK promoter was inserted into the genomic fragment for negative selection. After the targeting vector was transfected into 129/Sv mice-derived embryonic stem cells, G418 and ganciclovir doubly resistant colonies were selected and screened by PCR. The targeted cell line was injected into C57BL/6 blastocysts, resulting in the birth of male chimeric mice. These mice were then backcrossed with C57BL/6 mice. The disruption of the *IPS-1* gene was confirmed by PCR for the long and short arms. The abolishment of IPS-1 mRNA expression was confirmed by real-time quantitative PCR (RT-qPCR).

Cells, viruses, and reagents

Wild-type (WT) and TICAM-1$^{-/-}$ mouse embryonic fibroblasts (MEF) were prepared from 12.5- to 13.5-d-old embryos. PV, strain Mahoney, was amplified in Vero cells, and the viral titer was determined by a plaque assay. Bone marrow (BM) cells were prepared from the femur and tibia. The cells were cultured in RPMI 1640 (Invitrogen, New York, NY) supplemented with 10% FCS, 100 μM 2-ME, and 10 ng/ml murine GM-CSF or the culture supernatant of NIH3T3 cells expressing M-CSF. After 6 d, cells were collected and used as bone marrow-derived dendritic cells (BM-DC) or BM-derived macrophages (BM-Mf). For the preparation of BM-DC and BM-Mf, the medium was changed every 2 d. Splenic DC and NK cells were isolated using the MACS system (Miltenyi Biotec, Auburn, CA).

Experimental infection of mice

Five- to 8-wk-old C57BL/6 female mice were used throughout this study. Mice of different genotypes were i.p. or i.v. infected with PV at the doses indicated. The viability of the infected mice was monitored for 2 wk. We collected sera from the mice at different time points to measure viral titers by a plaque assay and cytokine levels by an ELISA. To determine the tissue viral titer, mice were euthanized and organs were aseptically removed and frozen by liquid nitrogen. Because the organs were not perfused before organs were removed, virus titers were determined including blood. Specimens were homogenized in 2 ml PBS on ice, and titers were determined by a plaque assay.

ELISA

Culture supernatants of cells (10^5) seeded on 24-well plates or sera were collected and analyzed for cytokine levels with ELISA. ELISA kits for IFN-α and IFN-β were purchased from PBL Biomedical Laboratories. ELISA was performed according to the manufacturer's instructions.

qPCR

For qPCR, total RNA was extracted with TRIzol (Invitrogen), and 0.2–0.5 μg RNA was reverse-transcribed using a high-capacity cDNA transcription kit (Applied Biosystems, Piscataway, NJ) with random primers according to the manufacturer's instructions. qPCR was performed using a Step One real-time PCR system (Applied Biosystems).

In vivo blocking of NK activity

Mice (PVRtg and PVRtg/TICAM-1$^{-/-}$) were i.p. injected with 250 μg anti-NK1.1 Ab, asialoGM1 Ab, or control PBS as described previously (21). One day later, the mice were i.p. inoculated with 10^4 PFU PV. One to 7 d after PV injection, depletion of peripheral NK1.1$^+$ cells was confirmed by flow cytometry. Then, the mortality of the mice was monitored. In some experiments, the spleen cells were harvested and NK cells (DX5$^+$ cells) were positively isolated using the MACS system (Miltenyi Biotec). The DX5$^+$ NK cells were suspended in RPMI 1640 containing 10% FCS and mixed with ^{51}Cr-labeled B16D8 cells at the indicated E:T ratios. After 4 h, the supernatants were harvested and [^{51}Cr] release was measured.

Statistical analysis

Statistical significance of differences between groups was determined by the Student *t* test, and survival curves were analyzed by the log-rank test using Prism 4 for Macintosh software (GraphPad Software). Student *t* tests and χ^2 goodness-of-fit tests were performed using Microsoft Excel software and a χ^2 distribution table.

Results

TICAM-1 is essential for protection of PVRtg mice against PV infection

Mice lacking the *mda-5* gene abrogate the production of type I IFN in response to EMCV infection and are more susceptible to infection with EMCV (13, 17). Because EMCV is a picornavirus, it has been proposed that MDA5 is critical for sensing picornavirus infection. In infected cells, picornaviruses efficiently generate long dsRNA, which is recognized by the cytoplasmic dsRNA sensor MDA5 (23). The 5′ end of the PV genomic RNA is linked to a VPg protein (16), not to a 5′-triphosphate, a major ligand for another cytoplasmic RNA sensor, RIG-I (24, 25). Thus, we first tested, using the PVRtg mouse model (20), whether the mortality of PV-infected mice is affected by disruption of IPS-1 (Fig. 1*A*). Approximately 70% of WT (PVRtg) mice and ~40% of IPS-1$^{-/-}$ mice survived >10 d postinoculation at an i.p. dose of 2×10^4 PFU. No statistical significance between these two groups was detected (Fig. 1*A*). In the same experiments, TICAM-1$^{-/-}$ mice died within 5 d by paralysis (Fig. 1*B*).

We next investigated the effect of the route of PV infection on mortality in this mouse model. PV (2×10^3 PFU) was injected i.p. or i.v. into WT and TICAM-1 mice and their mortality was examined (Fig. 1*C*, 1*D*). All TICAM-1$^{-/-}$ mice died by paralysis within 7.5 d irrespective of the injection route. The significance of this early mortality rate of PV-infected TICAM-1$^{-/-}$ mice was supported by statistical analysis. The mortality rates were slightly high in WT mice compared with IPS-1$^{-/-}$ mice when PV loads in mice were not very high (Supplemental Fig. 1*A*). This tendency seemingly diminished by early death of IPS-1$^{-/-}$ mice with high doses of PV input. These data suggested that TICAM-1, rather than IPS-1 (or the sensors RIG-I and MDA5), is a critical factor in protecting mice from PV-mediated paralytic death. This conclusion was confirmed using RIG-I$^{-/-}$ and MDA5$^{-/-}$ mice with a PVRtg background (S. Abe, K. Fujii, and S. Koike, submitted for publication).

These results showed a discrepancy with previous indications that MDA5 is critical in picornavirus protection (13). We therefore tested the dose dependence of PV in the survival of WT versus TICAM-1$^{-/-}$ mice. Surprisingly, high doses of PV (2×10^5 and 2×10^6 PFU) induced paralytic death in all WT as well as TICAM-1$^{-/-}$ mice within 6 d (Fig. 2*A*, 2*B*). Thus, high doses of PV (>2×10^5 PFU) appear to overpower the TICAM-1 PV-protective activity in vivo, which confirmed previous findings using other picornaviruses (13). TICAM-1 was most effective in

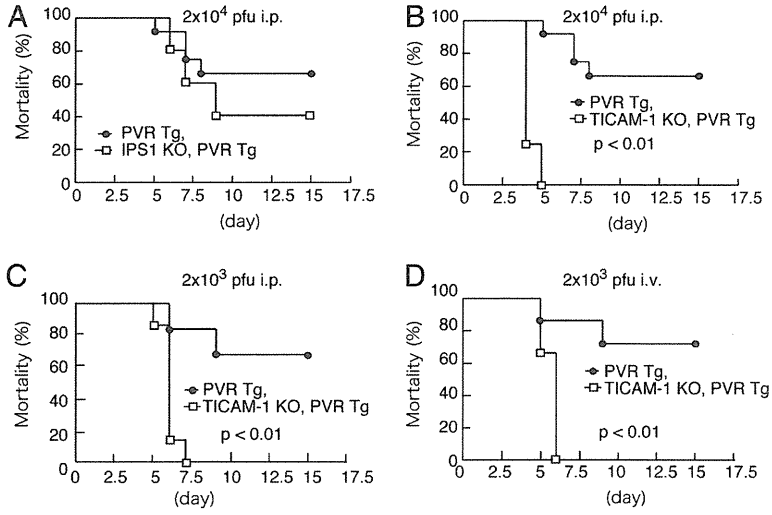

FIGURE 1. Survival of WT, TICAM-1 KO, and IPS-1 KO mice following i.p. or i.v. PV infection. *A* and *B*, PV (2×10^4 PFU) was infected via the i.p. route into WT and IPS-1 (*A*) or TICAM-1 (*B*) KO mice ($n \geq 5$), and survival was monitored for 14 d. *C* and *D*, PV (2×10^3 PFU) was infected via the i.p. (*C*) or i.v. (*D*) route into WT and TICAM-1 KO mice ($n \geq 5$), and survival was monitored for 14 d.

the survival against PV infection at low dose ($<2 \times 10^4$ PFU) (Figs. 1*B*, 1*C*, 2*C*). Similar results were obtained with the PV infection study (S. Abe, K. Fujii, and S. Koike, submitted for publication) when TICAM-$1^{-/-}$ mice were substituted with TLR3$^{-/-}$ or IRF-3/7 double-knockout (KO) mice. Results were confirmed using IRF-3$^{-/-}$ and IRF-7$^{-/-}$ mice (26). These results are essentially consistent with previous reports using a PVRtg/IFNAR$^{-/-}$ mouse model (27), in which type I IFN is critical for PV permissiveness, particularly in the intestine of PVRtg mice.

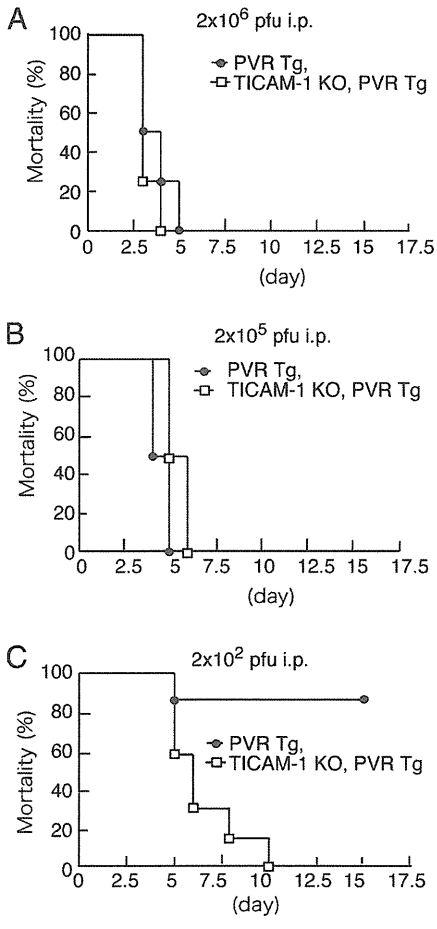

FIGURE 2. High doses of PV disable the protective effect of TICAM-1. WT and TICAM-1 KO mice ($n \geq 6$) were i.p. infected with 2×10^6 (*A*), 2×10^5 (*B*), or 2×10^2 PFU (*C*) PV and survival was monitored for 14 d.

TICAM-1–dependent type I IFN induction in PVRtg mice

PV titers in various organs were measured with WT and TICAM-$1^{-/-}$ mice i.p. injected with 2×10^4 PFU PV. In most organs, PV titers were higher in TICAM-$1^{-/-}$ mice than in WT mice at day 3 post-infection (Fig. 3*A*). The PV titer ratio in TICAM-$1^{-/-}$ versus WT mice was also high in the lung (Fig. 3*A*). In most organs except for the large intestine, high PV titers were harvested in TICAM-$1^{-/-}$ mice compared with WT mice. The difference in local PV titers between WT and TICAM-$1^{-/-}$ mice was culminated in the lung and spinal cord (Fig. 3*A*). Serum PV titers were increased within 48 h

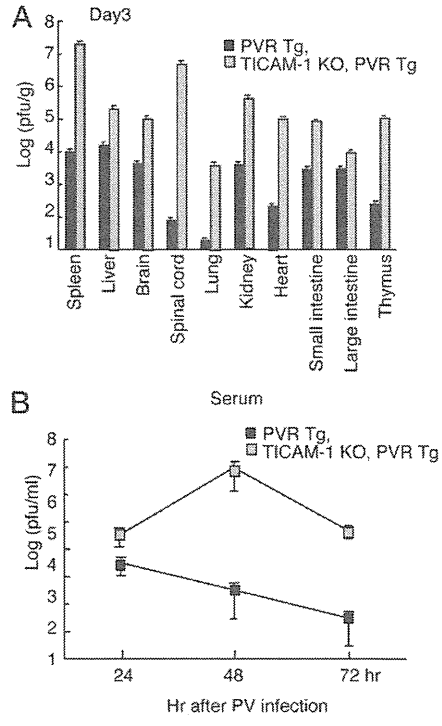

FIGURE 3. Viral titers in organs and serum following PV infection. WT and TICAM-1 KO mice were infected i.p. with 2×10^4 PFU PV. The viral titers in each organ (*A*) and sera (*B*) were measured by a plaque assay. Data are shown as means ± SD of three independent samples.

after PV i.p. injection in TICAM-$1^{-/-}$ mice compared with WT mice (Fig. 3*B*).

IFN-α/β levels were measured with sera from WT, IPS-$1^{-/-}$, and TICAM-$1^{-/-}$ mice, but they were barely detected in these PV-infected mice (Supplemental Fig. 1*B*). Only i.v. injection of high PV titers (an example shows $>4 \times 10^6$ PFU) allowed WT mice to release type I IFN within 12 h (Supplemental Fig. 1*B*). No IFN was detected in blood in TICAM-$1^{-/-}$ and IPS-$1^{-/-}$ mice even in this high-dose setting. However, IFN-α production was reproduced in a cell type level (peritoneal Mf) in vitro (Supplemental Fig. 1*C*). PV infection-mediated cell death (28) and degradation of MDA5 protein (29) may be major causes for this undetectable type I IFN production during in vivo PV infection.

TICAM-1 pathway contributes to IFN-β induction in WT mice with low PV titers

We next determined the mRNA levels of type I IFN in each organ extracted from PV (2×10^4 PFU)-infected WT and TICAM-$1^{-/-}$ mice. IFN-β mRNA was upregulated in all of the organs tested in WT mice within 12 h in response to PV injection (i.p.) (Fig. 4*A*). In contrast, only a low increase in IFN-β mRNA was detected in the organs of TICAM-$1^{-/-}$ mice (Fig. 4*A*). IFN-α2 mRNA was upregulated in the organs of TICAM-$1^{-/-}$ and WT mice to similar extents in response to PV injection (2×10^4 PFU, i.p.) (Fig. 4*B*). Notable decreases in IFN-α2 mRNA were observed in the TICAM-$1^{-/-}$ spleen and spinal cord compared with WT controls (Fig. 4*B*). The mRNA levels of genes associated with type I IFN induction were evaluated by qPCR, and no unique differences were observed between the splenocytes from PV-injected TICAM-$1^{-/-}$ and IPS-$1^{-/-}$ mice (Supplemental Fig. 1*D*). Hence, type I IFN mRNA is generally upregulated via TICAM-1 in the local organs of PVRtg WT mice during PV infection.

The mRNA levels of IFN-inducible genes and other cytokines were determined in spleen cells after PV infection. IFN-λ and IFN-γ–induced protein 10 (IP-10) mRNA were upregulated in the spleen cells of WT, but not TICAM-$1^{-/-}$ mice, after PV infection (multiplicity of infection [MOI] of 1) (Fig. 4*C*), with profiles similar to that of IFN-β mRNA (Fig. 4*C*). A sensor for 5′-triphosphorylated RNA, IFN-induced protein with tetratripeptide repeats 1 (IFIT-1), was also upregulated through PV infection (Fig. 4*C*). TNF-α, IL-10, IL-12p40, and IFN-γ, which may be associated with infectious cell death, were barely upregulated in spleen cells in response to PV infection (Supplemental Fig. 1*E*).

TICAM-1–dependent type I IFN induction by PV depends on Mf in PVRtg mice

The types of cells that participate in type I IFN induction in the spleen were examined by sorting spleen cells. IFN-β and IFN-α2 were found to be induced in WT $CD11c^+$ DC (Fig. 5*A*), whereas $CD11c^-$ cells barely induced type I IFN. Furthermore, IFN-β and IFN-α2 were barely induced in TICAM-$1^{-/-}$ $CD11c^+$ cells (Fig. 5*B*). Participation of IPS-1 in type I IFN induction in $CD11c^+$ myeloid cells is less compared with that of TICAM-1 (Fig. 5*B*).

Splenic $CD8\alpha^+CD11c^+$ and $CD4^+CD11c^+$ cells were separated by MACS beads and their response to PV (MOI of 1) was analyzed by determining the mRNA levels of type I IFN (Fig. 5*C*). $CD8\alpha^+CD11c^+$ cells, but not the $CD4^+CD11c^+$ cells, of WT mice were responsible for type I IFN induction by PV. There was a $CD4^-CD8\alpha^-$ population of DC in the spleen and this type of cells did not induce type I IFN in response to PV (Supplemental Fig. 2). The generation of the mRNA of type I IFN and IFIT-1 by PV infection was abrogated in the TICAM-$1^{-/-}$ $CD8\alpha^+CD11c^+$ splenic DC (Fig. 5*D*). Also, CD4/8α double-negative DC failed to express type I IFNs (Supplemental Fig. 2). Thus, $CD8\alpha^+CD11c^+$ DC, which reportedly express TLR3 (30), are the source of type I IFN in PV-infected PVRtg mice.

We finally confirmed that type I IFN is locally induced in $TLR3^+$ myeloid cells during PV infection. BM-Mf and BM-DC were prepared from mouse BM and challenged with PV (MOI of 1). These cells express TLR3 in the endosome as previously reported about mouse BM-DC (30) and human monocyte-derived DC (31). BM-Mf showed similar profiles of type I IFN mRNA to those of PV-infected splenocytes (Figs. 4*C*, 6*A*). However, IFN-λ and IP-10 mRNA were not detectable in PV-infected BM-Mf, the reason for which remains unclear (Fig. 6*A*). IL-12p40, a representative TICAM-1–dependent gene, was transiently upregulated

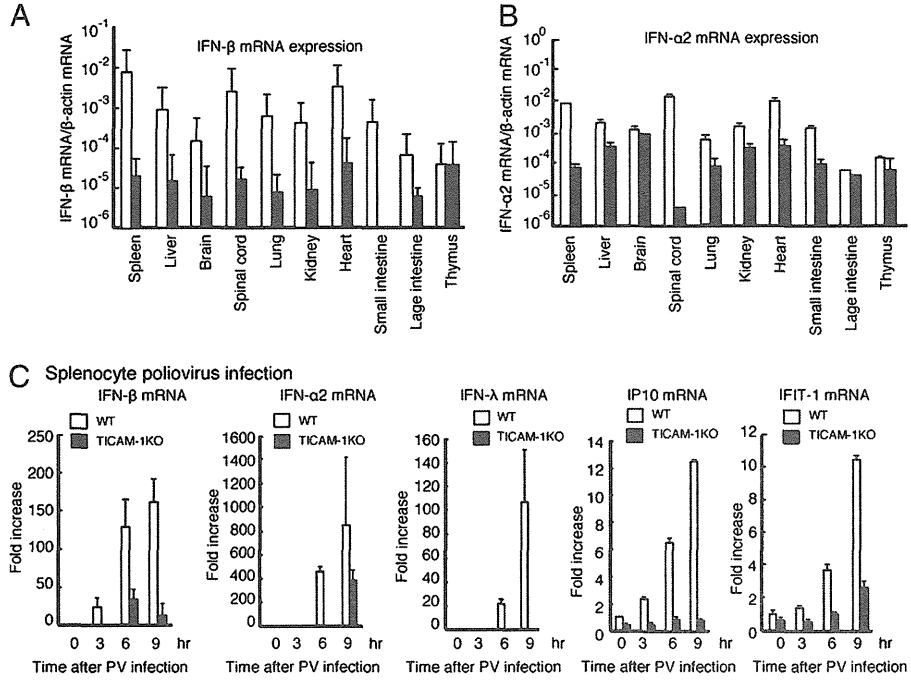

FIGURE 4. The expression of type I IFN following PV infection. *A* and *B*, WT and TICAM-1 KO mice were infected i.p. with 2×10^4 PFU PV. Three days postinfection, the mRNA expression levels of IFN-β (*A*) and IFN-α (*B*, *C*) were determined by RT-qPCR. *C*, Splenocytes (5×10^5) were infected with PV (MOI of 1) and the mRNA expression levels of IFN-β, IFN-α2, IFN-λ, IP-10, and IFIT-1 were measured by RT-qPCR. Data are shown as means ± SD and are representative of three independent experiments.

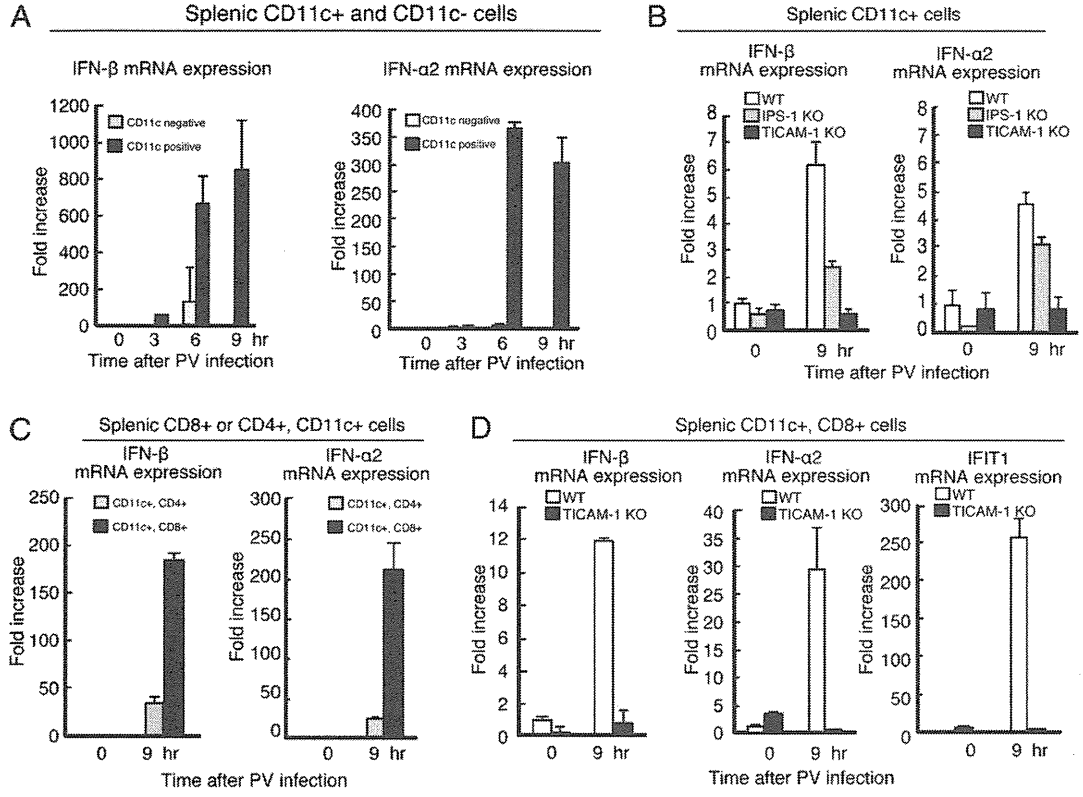

FIGURE 5. The expression of type I IFN in splenic DC. *A*, were isolated from WT spleens using the MACS system. $CD11c^+$ or $CD11c^-$ cells (5×10^5) were infected with PV (MOI of 1), and the mRNA expression of type I IFNs was measured by RT-qPCR. *B*, WT, TICAM-1, and IPS-1 knockout splenic $CD11c^+$ cells were infected with PV, and the expression of type I IFNs was measured by RT-qPCR. *C*, $CD8\alpha^+CD11c^+$ cells and $CD4^+CD11c^+$ cells were isolated from WT spleens and infected with PV (MOI of 1). The expression of type I IFNs was measured by RT-qPCR. *D*, $CD8\alpha^+CD11c^+$ splenic cells were isolated from WT and TICAM-1 KO mice and infected with PV (MOI of 1). The expressions of type I IFNs and IFIT-1 were measured by RT-qPCR. Data are shown as means ± SD and are representative of three independent experiments.

in BM-Mf ~4 h after PV infection (Supplemental Fig. 3). Similarly, but less prominently, the profiles of type I IFN and IL-12p40 were observed in BM-DC (Fig. 6*A*, Supplemental Fig. 3) and $CD11c^+CD8^+$ splenic DC (Fig. 5*D*). Therefore, taken together, these results indicate that IL-12 and IFN-α/β are only minimally upregulated in splenic DC in a PV-dependent manner.

The production of IFN-α was determined by ELISA in the supernatant of PV-infected BM-Mf and BM-DC (Fig. 6*C*). BM-Mf prepared from WT mice generated higher amounts of IFN-α than did those from TICAM-$1^{-/-}$ mice. Although similar results were obtained with BM-DC, the effect of TICAM-1 depletion was not statistically significant (Fig. 6*C*).

NK cells and MEF do not play major roles in protection against PV infection

Using NK1.1-depleted mice, we tested the possible participation of NK cells in the protection of PVRtg mice from PV infection (Fig. 7). $NK1.1^+$ cells were depleted from mouse blood 1 d after injection (i.p.) of NK1.1 Ab into WT (Fig. 7*A*) and TICAM-$1^{-/-}$ mice. After PV challenge, WT mice inoculated with control saline and NK1.1 Ab survived similarly, whereas TICAM-$1^{-/-}$ mice were all killed by PV within 7.5 d irrespective of NK1.1 pretreatment (Fig. 7*B*). Hence, NK cell activation does not affect PV-derived death. The lack of TICAM-1 was also found to have no effect on the NK cell-mediated rescue of PV-infected mice.

Mouse fibroblasts are known to be a potential source of type I IFN (13). We therefore checked whether MEF induce type I IFN and protection against PV (Supplemental Fig. 4). MEF from WT PVRtg mice were susceptible to PV, with cell death being observed at an MOI of 1. MEF from TICAM-$1^{-/-}$ PVRtg mice were 1 log more susceptible to PV, with cell death occurring at an MOI of 0.1 (Supplemental Fig. 4*A*). IFN-β was upregulated in PV-infected MEF to only a slightly higher level in PVRtg MEF than in TICAM-$1^{-/-}$ PVRtg MEF (Supplemental Fig. 4*B*). These results suggested that the large difference in the PV survival rate between WT and TICAM-$1^{-/-}$ mice is not caused by NK cells or type I IFN induction by fibroblasts. The TICAM-1 pathway plays a key role for producing IFN-α/β in Mf/DC, but not in fibroblasts, during PV infection in PVRtg mice.

Discussion

In this study, we demonstrated that PV infection is exacerbated in TICAM-$1^{-/-}$ PVRtg mice. There are a number of RNA-sensing molecules that serve as anti-virus agents and function in a cell type-specific manner. Based on trials using gene-disrupted mice and human viruses, RIG-I has been reported to be essential for sensing infection by rhabdoviruses, influenza viruses, paramyxoviruses, and flaviviruses, whereas MDA5 is important for sensing picornavirus infection (13, 33). In previous studies on picornaviruses, however, only EMCV and several species of picornaviruses have been employed for the KO mice analyses (13). The essential role of type I IFN in PV tropism has been well characterized in PVRtg mice (34). To our knowledge, this study is the first to investigate the sensor that detects PV infection in PVRtg PV-sensitive mice. Because RIG-I and MDA5 use the adaptor IPS-1, we constructed an IPS-$1^{-/-}$ mouse strain for this

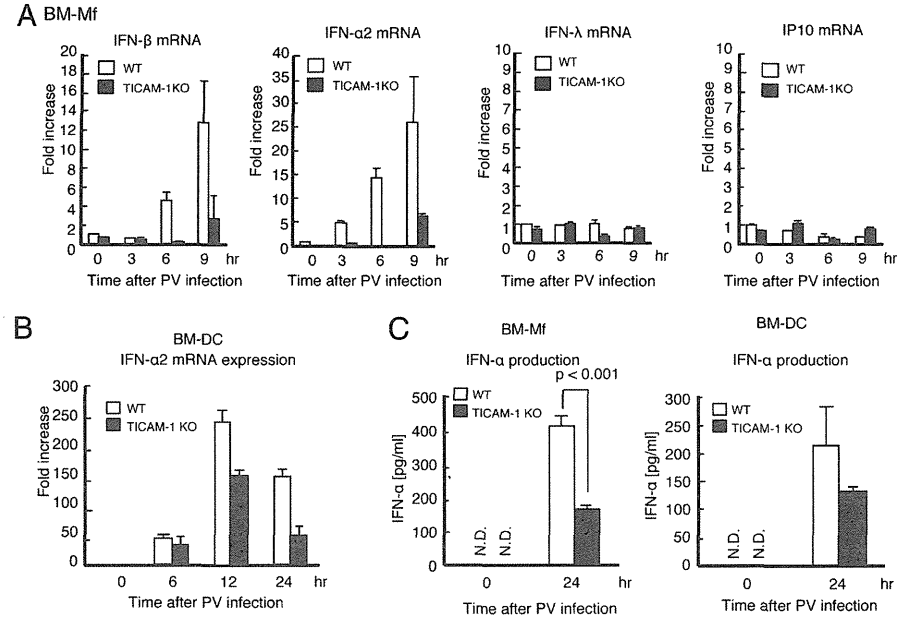

FIGURE 6. Production of type I IFN from BM-Mf and BM-DC. BM-Mf (*A*) and BM-DC (*B*) were prepared from BM cells with M-CSF and GM-CSF, respectively (32). The cells were infected with PV (MOI of 1), and the expression levels of IFN-β, IFN-α2, IFN-λ, and IP-10 were determined by RT-qPCR. *C*, IFN-α produced by PV-infected BM-Mf and BM-DC was measured by ELISA. BM-Mf and BM-DC were prepared from BM cells of WT and TICAM-1$^{-/-}$ mice as in *A* and *B*. Data are shown as means ± SD and are representative of three independent experiments.

study. Unexpectedly, however, IPS-1 was dispensable for protection against PV infection in vivo. This study, taken together with other reports (33, 35, 36), suggests that each virus species has its own strategy to evade host immune attack. This is true even in picornavirus subspecies. Although the IPS-1 pathway involving RIG-I and MDA5 is important for sensing and preventing cytoplasmic virus replication, other steps also participate in critical regulation of virus replication. PV infection is the case where MDA5 is not absolutely critical, but TICAM-1 is essential, for virus protection.

The TICAM-1 pathway participates in driving NK/CTL activation in DC/Mf (21, 37). This pathway is involved in type I IFN induction, as in the IPS-1 pathway, but cells expressing TLR3 are limited. The TLR3 distribution profile by flow cytometry confirms its expression in myeloid cells in mice (30). The TICAM-1 pathway converges with the IPS-1 pathway via the molecular complex of IRF-3–activating kinases (38), and therefore activation of the TICAM-1 pathway induces type I IFN and other IFN-inducible genes (39). Nevertheless, gene induction profiles differ between the TICAM-1 and IPS-1 pathways (40), which may explain the functional distinction between the sensor that is triggered in the virus-infected cells (MDA5/IPS-1) and the sensor that is required for DC/Mf to mount immune responses. Studying these gene functions will be an important issue for functional discrimination between the intrinsic versus extrinsic sensors.

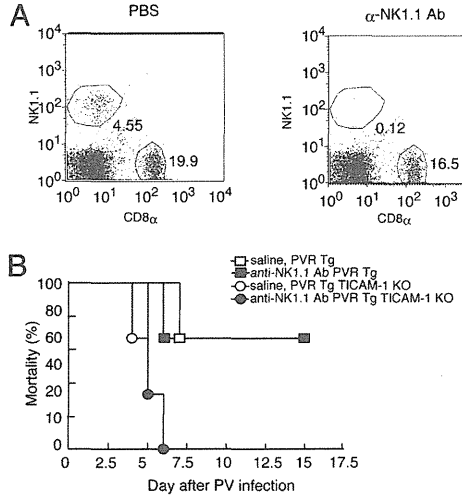

FIGURE 7. Effect of NK cells on mortality of PV-infected TICAM-1$^{-/-}$ PVRtg mice. *A*, To block the NK cell activity in mice, NK1.1 Ab or PBS (control) was i.p. injected into WT mice ($n \geq 6$). After 24 h, spleen cells were isolated from the mice and the fraction of NK1.1$^+$ cells was measured by FACS analysis. *B*, NK1.1 Ab or PBS was i.p. injected into WT and TICAM-1 KO mice. After 24 h, the mice were infected i.p. with PV, and survival was monitored for 15 d.

RIG-1/MDA5 are distributed over almost all organs, including Mf/DC. An interesting point concerns what the function is of the IPS-1 pathway in Mf/DC. Without conditional KO mice, we have an experimental limit to discriminate between their intrinsic function that is triggered in PV-infected cells and the extrinsic function leading Mf/DC to driving the innate immune response. Because the TLR3/TICAM-1 pathway is conserved in Mf/DC, the CNS, fibroblasts, and epithelical cells, it is reasonable that their functions are rather specified in Mf/DC and the neuronal system in PV infection.

However, except several examples such as rhabdovirus (41) and hepatitis C virus (HCV) (32), no definitive evidence has been reported supporting the role of TLR3/TICAM-1 in anti-RNA virus function using KO mice, unlike IPS-1 (35, 36). In previous studies, we used RNA viruses and their mouse models of measles virus, respiratory syncitial virus, vesicular stomatitis virus, influenza virus, and rotavirus infection (12), but we were unable to demonstrate solid antiviral function of the TLR3/TICAM-1 pathway in these models (12). Accordingly, which type I IFN, IFN-inducible gene, NK cell, or CTL is an effector for antagonizing viral replication still remains uncharacterized. To our knowledge, the results of our present study first demonstrated that the TLR3/TICAM-1 pathway is indispensable for induction of the type I IFN effector, but not NK cell activation, which is a critical event in the elimination of virus-infected cells and host protection against PV. IL-12 and IFN-γ are not upregulated in splenic DC in a PV-dependent manner. Furthermore, CTL are unlikely to be involved in our present model, since they would not function within the time scale of several days after initial infection (42).

How PV circumvents host-inducible type I IFN is an intriguing point. Three lines of evidence have supported the presence of unique mechanisms by which PV infection abrogates MDA5-mediated type I IFN production by infected cells and accelerates TLR3-mediated DC maturation through phagocytosis of PV-infected cell debris. First, proteases encoded in the PV genome process the PV polyprotein to produce functional viral proteins (43). PV 2A and 3C proteases also contribute to the degradation of eIF4G (44) and TATA-binding protein (45), respectively, the cleavage of which induces the translational and transcriptional "shutoff" of host protein synthesis (28). Thus, blocking the synthesis of host cell proteins by PV involves stopping IFN production. Second, MDA5 is degraded in PV-infected cells in a proteasome- and caspase-dependent manner, resulting in the lack of type I IFN production (29). Third, PV-mediated apoptosis occurs in a caspase-dependent manner to disable infected cells from inducing an IFN response (46), with the MDA5-dependent innate response to PV infection becoming minimal within 3 h postinfection. Additionally, RIG-I is also cleaved by the viral protease 3C (47), and additional RIG-I functions are subsequently disrupted. Hence, the RIG-I/MDA5 functional time frames should be narrow and ineffective in PV-infected cells.

The hijacked cells release virions and die irrespective of blocking of the IPS-1 pathway. These infected cells are degrading into apoptotic debris containing virus dsRNA when RIG-I/MDA5 is ineffective at inducing IFN (48). Phagocytic internalization of this infected debris containing viral dsRNA into endosomes in Mf/DC is a critical event for TLR3 stimulation (37). If this is the case in PV-infected PVRtg mice, dsRNA-containing debris produced by apoptosis of PV-infected cells may play a major role in the activation of the TICAM-1 pathway in myeloid cells, as is the case for another positive-stranded RNA virus, HCV (32). In HCV studies, dead cells act as carriers of viral dsRNA to the endosomes of DC (32). HCV induces cellular immunity including NK activation driven by the DC TICAM-1 pathway. PV, however, barely induces NK cell activation.

The results of the present study were obtained using the PVRtg mouse model for human PV infection. Possible limitations of this model may include the fact that PV natural infection in humans occurs postinfection of the intestine by a low dose of PV and the PV mouse model is unable to reproduce this infectious route (27). The difference in PV infection between human and the PVRtg mouse might reflect the difference of the IFN-inducing system in humans and mice. However, the response to neurovirulence and death by PV infection occurs similarly in mice and humans. PVRtg mice are susceptible to neuronal infection and the IFNAR$^{-/-}$ phenotype further enhances systemic PV infection (27, 34). The G (Sabin vaccine) and A forms (WT) of PV, which harbor G or A residues in their stem-loop V structures, respectively, show different levels of toxicity or neurovirulence (49). The lower toxicity of the vaccine strain is due to suppression of PTB-mediated protein synthesis in the G form. These results are essentially reproducible in the PVRtg mouse model (50). Our findings further indicate the essential role of the TICAM-1 pathway in the PVRtg model system for the PV-mediated induction of type I IFN in vivo. How this finding is associated with PV-mediated paralytic death and aberrance in the neuronal system is an open question for further understanding the PV neurovirulence and host defense.

In studies on virus infection in neurons, there was no difference between TLR3$^{-/-}$ and WT mice in the brain of reovirus infection (51). TLR3$^{-/-}$ mice have less severe neuroinvasiveness and survive longer than do WT mice in rabies virus infection (41). Further extensive studies have been performed with West Nile virus (WNV). TLR3$^{-/-}$ or TICAM-1$^{-/-}$ mice became more resistant to WNV infection than did WT mice (52). Compared to these earlier results, a recent report showed that lack of TLR3 enhances WNV mortality and increases viral burden in the brain (53). TNF-α and IL-6 are induced for inflammation, and high IL-10 production causes an increase of mortality in WNV-infected mice (54). TICAM-1 signaling is undoubtedly involved in the modulation of these cytokine productions and WNV replication in the nervous system (53, 54). In patients with herpes simplex encephalitis, functional deficiency of TLR3 or TICAM-1 is a critical factor for disease progression (55). The TLR3 responses in the CNS may differ from those in the immune system we examined (54, 56). How PV infection modulates IFN/cytokine-inducing signaling in the nervous system is an interesting issue. The possibility remains that cytokines, such as TNF-α, IL-10, IL-12p40, and IFN-γ, might be associated with the removal of infectious cells as in other virus infections, and the antiviral function of TLR3 ligands in PV-infected mice requires further elucidation.

A picornavirus CBV activates the TLR3/TICAM-1–IFN-γ axis in host-infected cells to induce type II IFN (18). It is possible that CBV promotes TLR3-dependent IFN-γ induction in lymphocytes rather than the type I IFN-inducing pathway. In the model of PV infection, however, the TICAM-1 pathway does not contribute to type II IFN induction. These findings indicate that picornaviruses, that is, EMCV, CBV and PV, have independently evolved to adapt to the host innate immune system and cope with the IFN-inducing system. If this is the case, host responses against picornaviruses may not be unimodally raised by MDA5 but may provide differentially adapted strategies. EMCV tropism reported previously (13) is clearly distinct from those of other picornaviruses. In this article, we present evidence that PV infection is protected by the TICAM-1 pathway that extrinsically induces type I IFN. Virus-produced dsRNA may differentially act on host cells depending on each virus species and accomplish circumvention from host innate sensing systems, maintaining virus tropism.

Acknowledgments

We are grateful to Dr. A. Nomoto (University of Tokyo, Tokyo, Japan) and our laboratory members for invaluable discussions. We also thank Dr. D.M. Segal (National Institutes of Health, Bethesda, MD) for providing us with anti-monse TLR3 mAb and Drs. S. Akira (Osaka University, Osaka, Japan) and T. Taniguchi (University of Tokyo) for providing TLR3$^{-/-}$ and IRF3/7$^{-/-}$ mice, respectively, for this study.

Disclosures

The authors have no financial conflicts of interest.

References

1. Takeuchi, O., and S. Akira. 2009. Innate immunity to virus infection. *Immunol. Rev.* 227: 75–86.
2. Malathi, K., B. Dong, M. Gale, Jr., and R. H. Silverman. 2007. Small self-RNA generated by RNase L amplifies antiviral innate immunity. *Nature* 448: 816–819.
3. Oshiumi, H., M. Matsumoto, K. Funami, T. Akazawa, and T. Seya. 2003. TICAM-1, an adaptor molecule that participates in Toll-like receptor 3-mediated interferon-β induction. *Nat. Immunol.* 4: 161–167.
4. Yamamoto, M., S. Sato, H. Hemmi, K. Hoshino, T. Kaisho, H. Sanjo, O. Takeuchi, M. Sugiyama, M. Okabe, K. Takeda, and S. Akira. 2003. Role of adaptor TRIF in the MyD88-independent Toll-like receptor signaling pathway. *Science* 301: 640–643.
5. Hoebe, K., X. Du, P. Georgel, E. Janssen, K. Tabeta, S. O. Kim, J. Goode, P. Lin, N. Mann, S. Mudd, et al. 2003. Identification of Lps2 as a key transducer of MyD88-independent TIR signalling. *Nature* 424: 743–748.
6. Akira, S. 2003. Toll-like receptor signaling. *J. Biol. Chem.* 278: 38105–38108.
7. Matsumoto, M., and T. Seya. 2008. TLR3: interferon induction by double-stranded RNA including poly(I:C). *Adv. Drug Deliv. Rev.* 60: 805–812.
8. Funami, K., M. Sasai, Y. Ohba, H. Oshiumi, T. Seya, and M. Matsumoto. 2007. Spatiotemporal mobilization of Toll/IL-1 receptor domain-containing adaptor molecule-1 in response to dsRNA. *J. Immunol.* 179: 6867–6872.
9. Funami, K., M. Sasai, H. Oshiumi, T. Seya, and M. Matsumoto. 2008. Homo-oligomerization is essential for Toll/interleukin-1 receptor domain-containing

adaptor molecule-1-mediated NF-κB and interferon regulatory factor-3 activation. *J. Biol. Chem.* 283: 18283–18291.
10. Yoneyama, M., M. Kikuchi, T. Natsukawa, N. Shinobu, T. Imaizumi, M. Miyagishi, K. Taira, S. Akira, and T. Fujita. 2004. The RNA helicase RIG-I has an essential function in double-stranded RNA-induced innate antiviral responses. *Nat. Immunol.* 5: 730–737.
11. Yoneyama, M., M. Kikuchi, K. Matsumoto, T. Imaizumi, M. Miyagishi, K. Taira, E. Foy, Y. M. Loo, M. Gale, Jr., S. Akira, et al. 2005. Shared and unique functions of the DExD/H-box helicases RIG-I, MDA5, and LGP2 in antiviral innate immunity. *J. Immunol.* 175: 2851–2858.
12. Matsumoto, M., H. Oshiumi, and T. Seya. 2011. Antiviral responses induced by the TLR3 pathway. *Rev. Med. Virol.* 21: 67–77.
13. Kato, H., O. Takeuchi, S. Sato, M. Yoneyama, M. Yamamoto, K. Matsui, S. Uematsu, A. Jung, T. Kawai, K. J. Ishii, et al. 2006. Differential roles of MDA5 and RIG-I helicases in the recognition of RNA viruses. *Nature* 441: 101–105.
14. Tabeta, K., P. Georgel, E. Janssen, X. Du, K. Hoebe, K. Crozat, S. Mudd, L. Shamel, S. Sovath, J. Goode, et al. 2004. Toll-like receptors 9 and 3 as essential components of innate immune defense against mouse cytomegalovirus infection. *Proc. Natl. Acad. Sci. USA* 101: 3516–3521.
15. Baltimore, D., Y. Becker, and J. E. Darnell. 1964. Virus-specific double-stranded RNA in poliovirus-infected cells. *Science* 143: 1034–1036.
16. Nomoto, A., B. Detjen, R. Pozzatti, and E. Wimmer. 1977. The location of the polio genome protein in viral RNAs and its implication for RNA synthesis. *Nature* 268: 208–213.
17. Gitlin, L., W. Barchet, S. Gilfillan, M. Cella, B. Beutler, R. A. Flavell, M. S. Diamond, and M. Colonna. 2006. Essential role of mda-5 in type I IFN responses to polyriboinosinic:polyribocytidylic acid and encephalomyocarditis picornavirus. *Proc. Natl. Acad. Sci. USA* 103: 8459–8464.
18. Negishi, H., T. Osawa, K. Ogami, X. Ouyang, S. Sakaguchi, R. Koshiba, H. Yanai, Y. Seko, H. Shitara, K. Bishop, et al. 2008. A critical link between Toll-like receptor 3 and type II interferon signaling pathways in antiviral innate immunity. *Proc. Natl. Acad. Sci. USA* 105: 20446–20451.
19. Ren, R. B., F. Costantini, E. J. Gorgacz, J. J. Lee, and V. R. Racaniello. 1990. Transgenic mice expressing a human poliovirus receptor: a new model for poliomyelitis. *Cell* 63: 353–362.
20. Koike, S., C. Taya, T. Kurata, S. Abe, I. Ise, H. Yonekawa, and A. Nomoto. 1991. Transgenic mice susceptible to poliovirus. *Proc. Natl. Acad. Sci. USA* 88: 951–955.
21. Akazawa, T., T. Ebihara, M. Okuno, Y. Okuda, M. Shingai, K. Tsujimura, T. Takahashi, M. Ikawa, M. Okabe, N. Inoue, et al. 2007. Antitumor NK activation induced by the Toll-like receptor 3-TICAM-1 (TRIF) pathway in myeloid dendritic cells. *Proc. Natl. Acad. Sci. USA* 104: 252–257.
22. Honda, K., H. Yanai, H. Negishi, M. Asagiri, M. Sato, T. Mizutani, N. Shimada, Y. Ohba, A. Takaoka, N. Yoshida, and T. Taniguchi. 2005. IRF-7 is the master regulator of type-I interferon-dependent immune responses. *Nature* 434: 772–777.
23. Kato, H., O. Takeuchi, E. Mikamo-Satoh, R. Hirai, T. Kawai, K. Matsushita, A. Hiiragi, T. S. Dermody, T. Fujita, and S. Akira. 2008. Length-dependent recognition of double-stranded ribonucleic acids by retinoic acid-inducible gene-I and melanoma differentiation-associated gene 5. *J. Exp. Med.* 205: 1601–1610.
24. Hornung, V., J. Ellegast, S. Kim, K. Brzózka, A. Jung, H. Kato, H. Poeck, S. Akira, K. K. Conzelmann, M. Schlee, et al. 2006. 5′-Triphosphate RNA is the ligand for RIG-I. *Science* 314: 994–997.
25. Pichlmair, A., O. Schulz, C. P. Tan, T. I. Näslund, P. Liljeström, F. Weber, and C. Reis e Sousa. 2006. RIG-I-mediated antiviral responses to single-stranded RNA bearing 5′-phosphates. *Science* 314: 997–1001.
26. Nakajima, A., K. Nishimura, Y. Nakaima, T. Oh, S. Noguchi, T. Taniguchi, and T. Tamura. 2009. Cell type-dependent proapoptotic role of Bcl2L12 revealed by a mutation concomitant with the disruption of the juxtaposed *Irf3* gene. *Proc. Natl. Acad. Sci. USA* 106: 12448–12452.
27. Ohka, S., H. Igarashi, N. Nagata, M. Sakai, S. Koike, T. Nochi, H. Kiyono, and A. Nomoto. 2007. Establishment of a poliovirus oral infection system in human poliovirus receptor-expressing transgenic mice that are deficient in α/β interferon receptor. *J. Virol.* 81: 7902–7912.
28. Racaniello, V. R. 2007. Picornaviridae: the viruses and their replication. In *Fields Virology*, 5th Ed. D. M. Knipe and P. M. Howley, eds. Lippincott Williams & Wilkins, Philadelphia, p. 795–838.
29. Barral, P. M., J. M. Morrison, J. Drahos, P. Gupta, D. Sarkar, P. B. Fisher, and V. R. Racaniello. 2007. MDA-5 is cleaved in poliovirus-infected cells. *J. Virol.* 81: 3677–3684.
30. Jelinek, I., J. N. Leonard, G. E. Price, K. N. Brown, A. Meyer-Manlapat, P. K. Goldsmith, Y. Wang, D. Venzon, S. L. Epstein, and D. M. Segal. 2011. TLR3-specific double-stranded RNA oligonucleotide adjuvants induce dendritic cell cross-presentation, CTL responses, and antiviral protection. *J. Immunol.* 186: 2422–2429.
31. Matsumoto, M., K. Funami, M. Tanabe, H. Oshiumi, M. Shingai, Y. Seto, A. Yamamoto, and T. Seya. 2003. Subcellular localization of Toll-like receptor 3 in human dendritic cells. *J. Immunol.* 171: 3154–3162.
32. Ebihara, T., M. Shingai, M. Matsumoto, T. Wakita, and T. Seya. 2008. Hepatitis C virus-infected hepatocytes extrinsically modulate dendritic cell maturation to activate T cells and natural killer cells. *Hepatology* 48: 48–58.
33. Loo, Y. M., J. Fornek, N. Crochet, G. Bajwa, O. Perwitasari, L. Martinez-Sobrido, S. Akira, M. A. Gill, A. García-Sastre, M. G. Katze, and M. Gale, Jr. 2008. Distinct RIG-I and MDA5 signaling by RNA viruses in innate immunity. *J. Virol.* 82: 335–345.
34. Ida-Hosonuma, M., T. Iwasaki, T. Yoshikawa, N. Nagata, Y. Sato, T. Sata, M. Yoneyama, T. Fujita, C. Taya, H. Yonekawa, and S. Koike. 2005. The α/β interferon response controls tissue tropism and pathogenicity of poliovirus. *J. Virol.* 79: 4460–4469.
35. Kumar, H., T. Kawai, H. Kato, S. Sato, K. Takahashi, C. Coban, M. Yamamoto, S. Uematsu, K. J. Ishii, O. Takeuchi, and S. Akira. 2006. Essential role of IPS-1 in innate immune responses against RNA viruses. *J. Exp. Med.* 203: 1795–1803.
36. Sun, Q., L. Sun, H. H. Liu, X. Chen, R. B. Seth, J. Forman, and Z. J. Chen. 2006. The specific and essential role of MAVS in antiviral innate immune responses. *Immunity* 24: 633–642.
37. Schulz, O., S. S. Diebold, M. Chen, T. I. Näslund, M. A. Nolte, L. Alexopoulou, Y. T. Azuma, R. A. Flavell, P. Liljeström, and C. Reis e Sousa. 2005. Toll-like receptor 3 promotes cross-priming to virus-infected cells. *Nature* 433: 887–892.
38. Sasai, M., M. Shingai, K. Funami, M. Yoneyama, T. Fujita, M. Matsumoto, and T. Seya. 2006. NAK-associated protein 1 participates in both the TLR3 and the cytoplasmic pathways in type I IFN induction. *J. Immunol.* 177: 8676–8683.
39. Oshiumi, H., M. Sasai, K. Shida, T. Fujita, M. Matsumoto, and T. Seya. 2003. TIR-containing adapter molecule (TICAM)-2, a bridging adapter recruiting to Toll-like receptor 4 TICAM-1 that induces interferon-beta. *J. Biol. Chem.* 278: 49751–49762.
40. Ueta, M., T. Kawai, N. Yokoi, S. Akira, and S. Kinoshita. 2011. Contribution of IPS-1 to polyI:C-induced cytokine production in conjunctival epithelial cells. *Biochem. Biophys. Res. Commun.* 404: 419–423.
41. Ménager, P., P. Roux, F. Mégret, J. P. Bourgeois, A. M. Le Sourd, A. Danckaert, M. Lafage, C. Préhaud, and M. Lafon. 2009. Toll-like receptor 3 (TLR3) plays a major role in the formation of rabies virus Negri bodies. *PLoS Pathog.* 5: e1000315.
42. Sigal, L. J., S. Crotty, R. Andino, and K. L. Rock. 1999. Cytotoxic T-cell immunity to virus-infected non-haematopoietic cells requires presentation of exogenous antigen. *Nature* 398: 77–80.
43. Nicklin, M. J., H. G. Kräusslich, H. Toyoda, J. J. Dunn, and E. Wimmer. 1987. Poliovirus polypeptide precursors: expression in vitro and processing by exogenous 3C and 2A proteinases. *Proc. Natl. Acad. Sci. USA* 84: 4002–4006.
44. Kräusslich, H. G., M. J. Nicklin, H. Toyoda, D. Etchison, and E. Wimmer. 1987. Poliovirus proteinase 2A induces cleavage of eucaryotic initiation factor 4F polypeptide p220. *J. Virol.* 61: 2711–2718.
45. Clark, M. E., P. M. Lieberman, A. J. Berk, and A. Dasgupta. 1993. Direct cleavage of human TATA-binding protein by poliovirus protease 3C in vivo and in vitro. *Mol. Cell. Biol.* 13: 1232–1237.
46. Belov, G. A., L. I. Romanova, E. A. Tolskaya, M. S. Kolesnikova, Y. A. Lazebnik, and V. I. Agol. 2003. The major apoptotic pathway activated and suppressed by poliovirus. *J. Virol.* 77: 45–56.
47. Barral, P. M., D. Sarkar, P. B. Fisher, and V. R. Racaniello. 2009. RIG-I is cleaved during picornavirus infection. *Virology* 391: 171–176.
48. Barco, A., E. Feduchi, and L. Carrasco. 2000. Poliovirus protease $3C^{pro}$ kills cells by apoptosis. *Virology* 266: 352–360.
49. Kawamura, N., M. Kohara, S. Abe, T. Komatsu, K. Tago, M. Arita, and A. Nomoto. 1989. Determinants in the 5′ noncoding region of poliovirus Sabin 1 RNA that influence the attenuation phenotype. *J. Virol.* 63: 1302–1309.
50. Koike, S., H. Horie, Y. Sato, I. Ise, C. Taya, T. Nomura, I. Yoshioka, H. Yonekawa, and A. Nomoto. 1993. Poliovirus-sensitive transgenic mice as a new animal model. *Dev. Biol. Stand.* 78: 101–107.
51. Edelmann, K. H., S. Richardson-Burns, L. Alexopoulou, K. L. Tyler, R. A. Flavell, and M. B. A. Oldstone. 2004. Does Toll-like receptor 3 play a biological role in virus infections? *Virology* 322: 231–238.
52. Wang, T., T. Town, L. Alexopoulou, J. F. Anderson, E. Fikrig, and R. A. Flavell. 2004. Toll-like receptor 3 mediates West Nile virus entry into the brain causing lethal encephalitis. *Nat. Med.* 10: 1366–1373.
53. Daffis, S., M. A. Samuel, M. S. Suthar, M. Gale, Jr., and M. S. Diamond. 2008. Toll-like receptor 3 has a protective role against West Nile virus infection. *J. Virol.* 82: 10349–10358.
54. Bai, F., T. Town, F. Qian, P. Wang, M. Kamanaka, T. M. Connolly, D. Gate, R. R. Montgomery, R. A. Flavell, and E. Fikrig. 2009. IL-10 signaling blockade controls murine West Nile virus infection. *PLoS Pathog.* 5: e1000610.
55. Zhang, S. Y., E. Jouanguy, S. Ugolini, A. Smahi, G. Elain, P. Romero, D. Segal, V. Sancho-Shimizu, L. Lorenzo, A. Puel, et al. 2007. TLR3 deficiency in patients with herpes simplex encephalitis. *Science* 317: 1522–1527.
56. Préhaud, C., F. Mégret, M. Lafage, and M. Lafon. 2005. Virus infection switches TLR-3-positive human neurons to become strong producers of beta interferon. *J. Virol.* 79: 12893–12904.

Figure S1

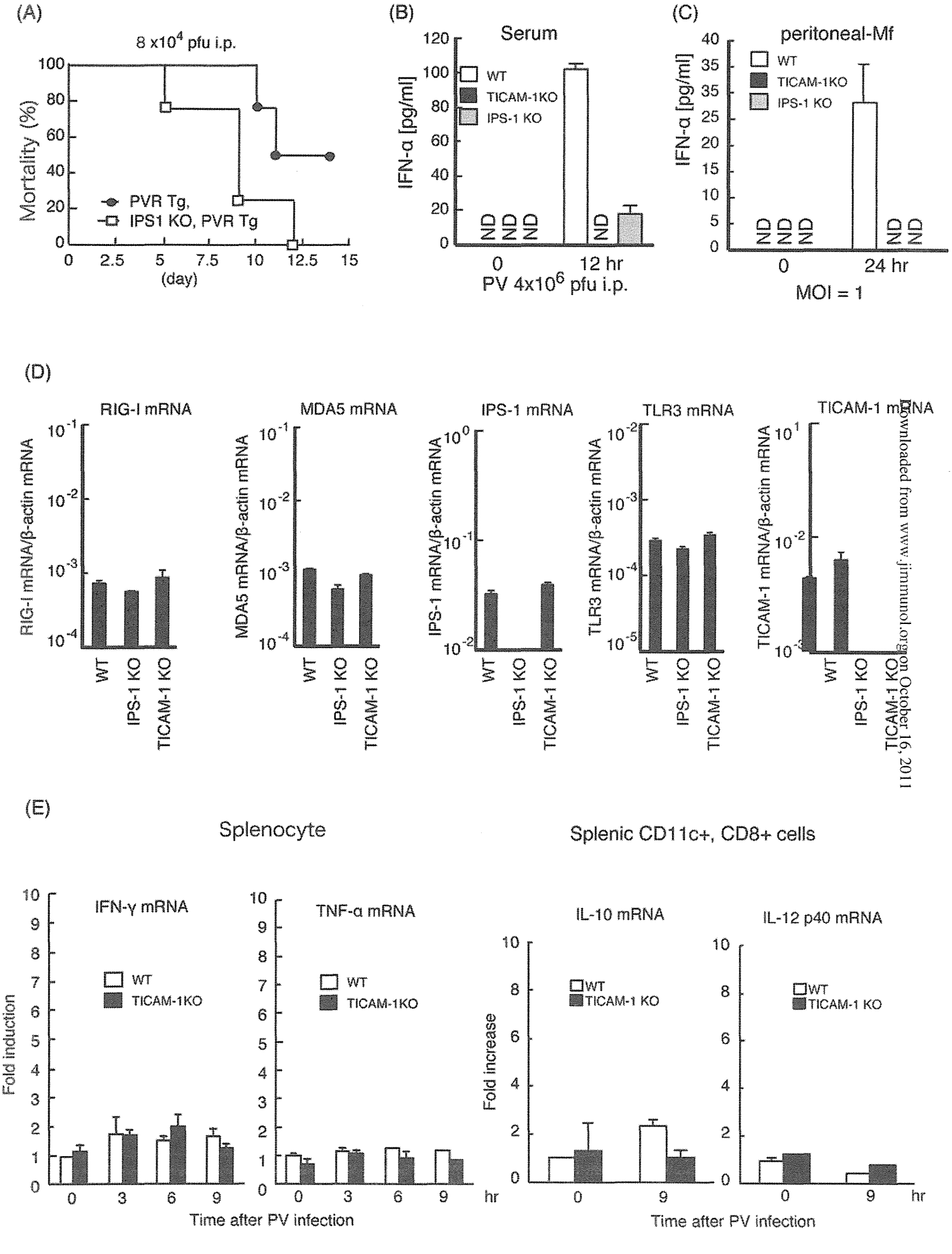

Figure S2

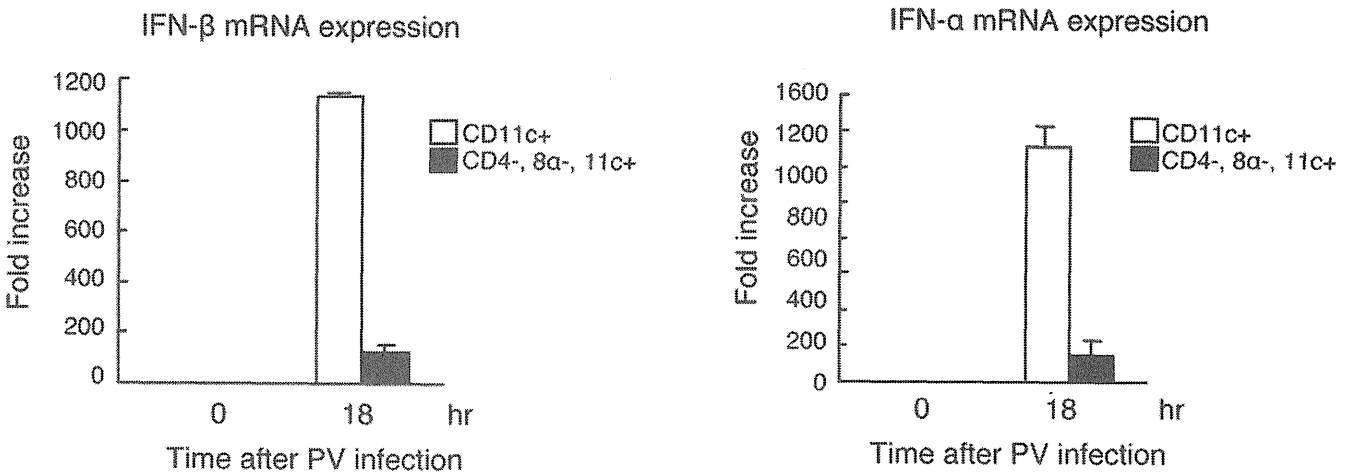

Figure S3